Research Square

Preprints are preliminary reports that have not undergone peer review.
They should not be considered conclusive, used to inform clinical practice,
or referenced by the media as validated information.

Multiomic Analysis of Cachectic Mice Reveals Cancer Driven Suppression of Muscle Differentiation

Vahab Soleimani

vahab.soleimani@uottawa.ca

University of Ottawa

Darren Blackburn

University of Ottawa

Aldo Hernández-Corchado

McGill University

Korin Sahinyan

McGill University

Hedieh Habibi Khorasani

University of Ottawa

Felicia Lazure

Moffitt Cancer Center

Vincent Richard

Lady Davis Institute

Dianbo Qu

University of Ottawa https://orcid.org/0000-0002-0435-9585

Shuo Wang

Christoph Borchers

Lady Davis Institute https://orcid.org/0000-0003-2394-6512

Arezu Jahani-Asl

University of Ottawa https://orcid.org/0000-0003-4002-3381

Hamed Najafabadi

McGill University https://orcid.org/0000-0003-2735-4231

Antonis Koromilas

McGill University https://orcid.org/0000-0003-1972-0799

Article

Keywords:

Posted Date: November 12th, 2026

DOI: https://doi.org/10.21203/rs.3.rs-10999038/v1

License: This work is licensed under a Creative Commons Attribution 4.0 International License.
Read Full License

Additional Declarations: (Not answered)

Multiomic Analysis of Cachectic Mice Reveals Cancer Driven Suppression of Muscle Differentiation

Darren M. Blackburn[1,*], Aldo Hernández-Corchado[2], Korin Sahinyan[2,3], Hedieh Habibi Khorasani[1], Felicia Lazure[4], Vincent Richard[5], Dianbo Qu[9], Shuo Wang[3] Christoph H. Borchers[5-8], Arezu Jahani-Asl[9], Hamed S. Najafabadi[2], Antonis E. Koromilas[3,6], Vahab D. Soleimani[1,2,*]

[1] *Department of Biochemistry, Microbiology & Immunology, University of Ottawa, 451 Smyth Rd, Ottawa, ON, K1H 8M5 Canada*

[2] *Department of Human Genetics, McGill University, 3640 rue University, Montréal, QC, H3A 0C7, Canada.*

[3] *Lady Davis Institute for Medical Research, Jewish General Hospital, 3755 Chemin de la Côte-Sainte-Catherine, Montréal QC, H3T 1E2, Canada.*

[4] *Moffit Cancer Center, Tumor Microenvironment and Metastasis Department, Tampa, FL 33612, USA.*

[5] *Segal Cancer Proteomics Centre, Lady Davis Institute, Jewish General Hospital, McGill University, Montréal, Quebec H3T 1E2, Canada.*

[6] *Gerald Bronfman Department of Oncology, Lady Davis Institute for Medical Research, Jewish General Hospital, Montréal, QC H3T 1E2, Canada*

[7] *Division of Experimental Medicine, McGill University, Montréal, QC H4A 3J1, Canada*

[8] *Department of Pathology, McGill University, Montréal, QC H3A 2B4, Canada*

[9] *Department of Cellular and Molecular Medicine and University of Ottawa Brain and Mind Research Institute, University of Ottawa, Ottawa, ON, Canada*

[*] *Corresponding authors: Vahab D Soleimani: Tel: +1 613 562 5409 ext. 7771, vahab.soleimani@uottawa.ca*

Darren M Blackburn: Tel: +1 613 809 1759, dblackb3@uottawa.ca

Abstract

Cancer cachexia is a severe wasting syndrome characterized by progressive loss of skeletal muscle mass, reduced regenerative capacity, and poor response to cancer therapy. The mechanisms by which tumors directly disrupt muscle stem cell function remain incompletely understood. Using the C26 adenocarcinoma model, we show that tumor cells undergo marked transcriptional adaptation within the host environment and acquire a secretory program that directly reprograms skeletal muscle and muscle stem cells. Multiomic profiling revealed that cachexia is associated with broad transcriptional and epigenetic remodeling of muscle stem cells, including induction of an epithelial-to-mesenchymal transition (EMT)-like program, reduced accessibility at myogenic regulatory factor binding sites, and impaired expression of key differentiation regulators. Mechanistically, exposure to the C26 tumor secretome increased SNAI1, a central EMT regulator, while suppressing MyoD, Myogenin, and MyHC and blocking myogenic differentiation and fusion. Importantly, SNAI1 knockdown rescued myogenic differentiation in the presence of C26-conditioned medium, establishing SNAI1 as a functional mediator of tumor-induced myogenic suppression. Cytokine profiling identified MMP9 as a prominent tumor-derived circulating factor, and pharmacological MMP9 inhibition in tumor-bearing mice preserved the PAX7-positive muscle stem cell pool. In contrast, loss of tumor-derived GDF15 alone was insufficient to rescue cachexia, supporting a multifactorial tumor-secretome model. Together, these findings define a mechanistic axis in which tumor adaptation to the host promotes induction of EMT-like reprogramming in muscle progenitors, suppresses myogenic differentiation, and contributes to regenerative failure and muscle wasting.

Introduction

Cancer cachexia is a debilitating condition where patients suffer a severe and rapid decline in muscle mass, with or without the loss of fat mass[1-3]. Muscle wasting is a common symptom in cancer, with approximately 80% of late-stage cancer patients exhibiting it[4]. Cachexia results in a worse prognosis for patients; they are less responsive to cancer therapies and suffer a loss of quality of life[1,5,6]. Furthermore, cachexia is itself responsible for approximately 30% of all cancer related death, primarily due to respiratory or heart failure[4]. Beyond muscle wasting, cancer cachexia is also associated with metabolic imbalance, systemic inflammation, insulin resistance, and anorexia[7-10]. It is a complex and multifactorial condition.

Cancer cachexia is not present in all cancers equally. It is more prevalent in gastrointestinal and pancreatic cancers, with between 60-70% of patients exhibiting muscle wasting[11]. However, it is much less common in breast cancer, with muscle wasting affecting nearly 20% of patients[11]. It is important to note, that the cancer does not need to be present in the muscle to induce muscle wasting. Other factors that affect the incidence of cachexia are the stage of the cancer; patients with advanced cancer are more likely to have cancer cachexia compared to those in earlier stages, as well as the sex of the patient[12]. Males are more susceptible to cancer cachexia, present in 61% of male patients in contrast to the 31% incidence in female patients[12,13].

Despite the severity and prevalence of the condition, there is no effective treatment or therapy for cachexia. Furthering our understanding on how the cancer cells alter skeletal muscle and muscle stem cell behaviour is necessary for the development of effective therapies. In this study, we sequenced the transcriptome of myofibers and muscle stem cells from healthy controls and tumor bearing male and female mice, identifying several key pathways that are deregulated. Muscle stem cells in cachectic mice exhibit delayed activation and a decrease in myogenic potential.

Additionally, we discovered how C26 cancer cells alter their transcriptome to adapt to the host environment. Specifically, we identify activation of SNAI1 and an epithelial-to-mesenchymal transition (EMT)-like transcriptional program in MuSCs from cachectic mice, which is associated with impaired myogenic differentiation and increased susceptibility to apoptosis. Functionally, SNAI1 depletion partially restores myogenic differentiation, while pharmacological inhibition of tumor-associated MMP9 preserves the MuSC pool in vivo, supporting a hypothesis in which SNAI1 is a downstream mediator of myogenic suppression and MMP9 acts as a potential upstream regulator. Cachexia is a debilitating condition in which the molecular mechanisms driving it are not well understood. Here, we conduct a comprehensive overview of the changes occurring in the skeletal muscle, and the resident MuSCs.

Results

C26 Tumors Induce Cachexia in Male and Female Mice

We used C26 adenocarcinoma cells, a highly aggressive cancer that is known to induce cachexia[14,15]. 3-month-old male and female Balb/c mice were given two subcutaneous injections of C26 cells at different locations of the body, and the tumor were allowed to grow until the mice reached endpoint, typically between the 2-and 3-week postinjection timepoint, and the muscle was collected for analysis (Fig. 1A).

To begin, we wanted to validate the findings that the C26 cells do indeed cause cachexia. We see that the C26 cells can quickly form large tumors in the mice (Fig. 1B) and that the female mice show a rapid and large loss in body weight (Fig. 1C), as well as a decrease in myofiber size (Fig. 1D,E). We analyzed male mice using an EchoMRI at their endpoint and found a dramatic decrease in the percentage of fat mass, with many of the mice reaching 0% (Fig. 1F). As a consequence of this loss of fat, there is a subsequent increase in the percentage of lean mass in the tumor bearing mice (Fig. 1G). This may seem contrary to what cachexia is, which is the loss of muscle mass with or without the loss of fat, but because these are percentages the loss of fat will cause the percentage of the lean mass to increase. It is also important to note that the tumor itself is measured primarily as lean mass in the EchoMRI. As a result, we see a large decrease in the tumor free body mass of these male mice (Fig. 1H).

Cachexia is associated with changes in diet and metabolism[16,17]. To quantify these changes, we housed male mice in metabolic cages for the entire period of tumor development, from tumor injection to endpoint. We see that within the first 2 weeks of tumor growth that there is no significant difference between the healthy controls and the tumor bearing mice with regards to food consumption (Fig. 1I,J). However, within the third week, we see a significant drop in the amount of food eaten by the tumor bearing mice (Fig. 1K). This is reflected in the energy metabolism as well. Within the first 2 weeks, there is no difference in the metabolism, with both conditions closer to a Respiratory Exchange Ratio (RER) of 1.0, indicating a preferential use of carbohydrates for their energy (Fig. 1L,M). Then in the third week, RER values in the cachectic mice drops towards 0.7 (Fig. 1N), indicating that they are starting to use more fat for energy, which may explain the loss of fat mass in these mice. Overall, we confirmed that the C26 cells that will be used in the rest of this study do induce cachexia.

Cancer Alters the Myofiber Transcriptome

Myofibers are the primary component of skeletal muscle, and they undergo atrophy in cachexia. However, to date, there has been no sequencing performed on only the myofibers to determine the transcriptomic changes that cachexia induces. To address this knowledge gap, we performed single myofiber RNA-Seq (smfRNA-Seq)[18] on individual myofibers isolated from healthy controls or tumor bearing mice, in both male and females (Fig. 2A). Specifically, a single EDL myofiber was isolated and sequenced from each of the 4 tumor bearing mice and 4 healthy control mice of each sex. To begin, we validate that every myofiber sequenced were fast type fibers by assessing the gene expression of key fast and slow myofiber genes. We see that every sequenced were fast type as evidenced by the exclusive expression of fast fiber type genes (i.e. Myh4, Tnnt3 and Tnni2) and the lack of expression of slow fiber type genes (i.e. Myh7, Tnnt1 and Tnni1) (Expanded View Fig. 1A) From the RNA-Seq results, we see that there is a large change in the myofiber transcriptome due to cancer, in both male and female mice (Fig. 2B,C). Using a threshold of LFC $\geq$ 1, adjusted p-value $\leq$ 0.05 and RPM $\geq$ 5 in at least one condition, we see in female myofibers that 770 genes are significantly downregulated, and 1154 genes are upregulated when comparing myofibers from healthy controls to those from tumor bearing mice (Fig. 2D,E). This is in contrast to male myofibers, where only 150 and 231 genes are significantly downregulated or upregulated, respectively (Fig. 2D,E).

The reason for this large discrepancy between the sexes could be due to the inherent variability between samples as each sequenced sample is that of an individual myofiber. We see that in PCA plots, the control and cachectic conditions do separate out from one another in both female and male samples (Fig. 2F,G) however in the Pearson Correlation heatmaps we do not see a strong division between control and cachexia samples (Fig. 2H). Because smfRNA-Seq is a single cell sequencing method, it is to be expected that there would be variation between samples. This variation would cause changes in gene expression to be less significant in terms of adjusted p-value, due to the spread of the samples. As such, it cannot be concluded from these data whether male or female muscle is more affected by cachexia.

A more in-depth analysis of the transcriptomic changes reveals that many key genes for myofiber function are deregulated in cachexia. Here, we highlight some genes selected from the top 20 most differentially expressed genes as ranked by adjusted p-value. There is an overlap between male and female myofibers. For example, PDK4, ACOT1 and ACOT2 are all in the top 20 most differentially expressed genes in both male and females (Fig. 2J-M). PDK4 inhibits pyruvate dehydrogenase, meaning it has a role glucose metabolism, and its overexpression may shift metabolism towards fatty acid oxidation[19]. ACOT1 and ACOT2 are genes that encode Acyl-CoA Hydrolase enzymes, which is important for fatty acid metabolism[20]. These findings indicate that there may be major changes in the metabolism of myofibers in cachexia. Female myofibers also showed a decrease in *Mafa* transcript, a key transcription factor in the maturation and maintenance of fast type myofibers (Fig. 2N)[21,22]. Male myofibers also have a significant decrease in *Mafa* expression, but it does not fall within the top 20 genes. Mafa is also known to promote the expression of Myh4[21], and we see in both male and female myofibers that Myh4 expression is decreased. Lastly, for the female myofibers, we observed a large increase in the expression of *Map1lc3b,* a gene that has a known function in autophagy (Fig. 2O)[23]. Looking at the top 20 most differentially expressed genes in male myofibers, we see that there is a near complete ablation of the expression of *Ampd1* (Fig. 2P). AMPD1 deficiency is a common mutation with a wide array of phenotypes, ranging from asymptomatic to exercise intolerance to muscle atrophy, however the more severe phenotypes cannot be attributed solely to mutations in the AMPD1 gene[24].

Interestingly, while *Ampd1* has lost almost all of its transcripts in males, in females there is only an approximate 40% loss of expression. We also see a considerable decrease in *Mrln* in male myofibers, but not in female myofibers (Fig. 2Q). This gene has a function in regulating Ca^{2+} uptake in the sarcoplasmic reticulum by inhibiting SERCA and its deregulation could cause defects in the ability of the myofiber to contract properly[25].

We performed a GSEA analysis between control and cachectic myofibers. We see in the females that among the most upregulated pathways there is Myc Targets V1, which are genes that are often activated as a response to cancer (Fig. 2R). There is also an enrichment in the Hypoxia pathway (Fig. 2R), which is known to induce muscle atrophy and inhibits myofiber growth[26]. When looking at the downregulated Hallmark pathways, we see that the 2 most enriched pathways are WNT Beta Catenin Signaling and NOTCH Signaling (Fig. 2S). Both signaling pathways are crucial for proper muscle function[27,28]. In males, many of the upregulated pathways are similar to the females, such as Hypoxia (Fig. 2T). However, their top pathway is Apoptosis (Fig. 2T), indicating that the myofibers may be undergoing cell death in cachexia. Interestingly, no downregulated pathways were significantly enriched in the male context. We wanted to compare how our results from mice contrasts with those from humans. A recent study by Judge et al. performed microarray on muscle biopsies from pancreatic ductal adenocarcinoma (PDAC) patients[14]. Using the publicly available data (GSE130563)[14] we performed a GSEA between the cachectic (n=17) and non cachectic (n=5) patients. We found that there was a large overlap between the pathways that are enriched in the human cachectic patients and the ones enriched in the mouse data. Notably, IL2 STAT5 Signaling, Apoptosis and KRAS Signaling Up (Fig. 2U). TNFA Signaling via NFKB, IL6 JAK STAT3 Signaling and Inflammatory response were also enriched but did not reach significance. These results indicate that there are common pathways that are deregulated between our mouse and human data.

There are known sex differences in muscle function, therefore we wanted to further explore any potential differences between male and female myofibers and how they respond to cachexia. We see that there is a large difference in the transcriptome between male and female myofibers, regardless of whether they are from healthy mice or cachectic mice (Expanded View Fig. 1B). At a threshold of LFC $\geq$ 1, adjusted p-value $\leq$ 0.05 and RPM $\geq$ 5 in at least one condition, there are 1039 genes that are upregulated in males and 451 that are downregulated (Expanded View Fig. 1B) in healthy myofibers. In cachectic myofibers, there are 789 and 516 genes are that upregulated and downregulated in males (Expanded View Fig. 1B). Interestingly, the majority of the top 100 differentially expressed genes are upregulated in the males (Expanded View Fig. 1C), this may be partially due to the Y chromosome genes, which are uniquely expressed in male cells. Through PCA analysis and Pearson Correlations, the samples tend to cluster more based on sex, while still showing a high degree of variability (Expanded View Fig. 1D-G).

A more in-depth analysis of the genes that are differentially expressed between male and female myofibers indicates, as expected, that the majority of the top DEGs in are those coded on the Y chromosome, such as Ddx3y and Eif2s3y (Expanded View Fig. 1H,I). However, not every top DEG is on the Y chromosome. For example, we see that ZFP280d, which is present on Chromosome 9, is very highly expressed in male myofibers in healthy controls, averaging at 1842 RPM, while in females it is mostly not expressed with an average RPM of 2.7 (Expanded View Fig. 1H). Very little is known about ZFP280d, to date no studies have been performed on its role in muscle. Interestingly, in cachexia, males lose expression of ZFP280d, with the average expression dropping to 208 RPM. Generally, we see that there is a positive correlation on the effect

of cachexia in both male and females. When all genes are considered, there is an r value of 0.2432, a modest correlation (Expanded View Fig. 1J). However, when we only plot genes that are significantly different in both comparisons, we see a much stronger correlation of r = 0.8435 (Expanded View Fig. 1K). As a whole, while there are differences on the effect of cachexia between male and female myofibers, the factor that more greatly explains their differences is sex itself.

An imbalance between protein synthesis and protein degradation is viewed to be a mechanism that causes the loss in muscle mass[29]. We wanted to assess the protein dynamics in whole muscle. To do so, we used heavy labelled amino acids to track the formation of new proteins during cachexia. In short, we treated Balb/c mice with heavy arginine in their drinking water for one week, after which the water was replaced with unsupplemented water. Two days later, the mice were injected with C26 cells, and the tumors were allowed to grow for 7 days. Afterwards, mice were then given water that had heavy lysine in it for another 7 days. The mice were then euthanized and the whole muscle and tumors processed for Mass Spec analysis.

From our results, we see that there is a distinct change in the proteome of cachectic mice compared to healthy controls, with the samples clustering separately on the PCA (Expanded View Fig. 2A). Pearson analysis also indicates that the cachectic muscle samples are more similar to each other than the controls (Expanded View Fig. 2B). However, we only detected 29 significantly different (LFC $\geq$ 1.5, adjusted p-value $\leq$ 0.05) proteins, and interestingly, most of them were upregulated (Expanded View Fig. 2C,D). This low number of significantly different proteins may be due to challenges in performing mass spectrometry on whole muscle as the structural proteins are very abundant. In our results, the top 20 most expressed proteins in the whole muscle, most of which are the myofiber structural genes, represent 50% of all detected peptides. Titin alone, which is the most highly expressed protein in the muscle, represents about 17% of all detected peptides in our results. This is in contrast to the whole tumor mass spec, where the top 20 proteins only represent about 18% of all detected peptides.

When quantifying the percentage of peptides containing the heavy amino acids, we see interesting results. To begin, the muscle from the control and the cachectic mice show the incorporation of an equal percentage of heavy amino acids. As expected, the first administered amino acid (arginine), was detected at lower levels and the second heavy amino acid was highly detected, indicating that the cachectic myofibers were still capable of incorporating the amino acid and therefore were producing new proteins (Expanded View Fig. 2E). However, the most interesting result from the Mass Spec data is that the tumor itself incorporated the heavy arginine, albeit at lower levels than the muscle, which was administered prior to tumor injection (Expanded View Fig. 2E). This suggests that the tumor cells are consuming the proteins from other tissues, most likely from the muscle as it is the protein storage of the body, however, as serum kinetics and tissue source tracing were not performed it cannot be definitively stated where the heavy arginine originates from.

Muscle Stem Cell Transcriptome is Greatly Altered in Cachexia

We have sequenced freshly isolated MuSCs from both male and female mice in 4-month-old healthy controls and tumor bearing mice (Fig. 3A). From these results, we see that there is a large change in the transcriptome of MuSCs due to cachexia (Fig. 3B,C). In female mice, at a threshold of LFC $\geq$ 1, adjusted p-value $\leq$ 0.05 and RPM $\geq$ 5 in at least one condition, MuSCs have 2185 genes down in cachexia and 2211 are upregulated (Fig. 3D,E). Males in contrast have 751 and 531

genes that are downregulated and upregulated, respectively (Fig. 3D,E). The MuSC samples cluster mostly based on cachexia in both males and females (Fig. 3F-I).

When comparing male and female MuSCs, we see that there is a lot of transcriptomic changes between the sexes (Expanded View Fig. 3A,B). The samples mostly cluster based on sex in both PCA plots and with Pearson Correlation, regardless of whether the sample came from healthy or cachectic mice (Expanded View Fig. 3C-F). We see that the most differentially expressed genes are typically Y chromosome genes (Expanded View Fig. 3G,H), as was seen when comparing male and female myofibers. We wanted to assess whether the effect of cachexia was similar between male and female MuSCs. Using scatterplots plotting the LFC of gene expressing between control and cachectic, we see a strong correlation between the sexes when looking at both all genes and just the significantly different genes (Expanded View Fig. 3I,J)

Looking more in depth at the changes due to cancer in the MuSC transcriptome, we see in females that among the top 20 genes that are most significantly different, that Col3a1 is greatly reduced in cachexia (Fig. 3J). Col3a1 is an essential ECM component of the MuSC niche, and its loss is associated with an increase in ECM stiffness[30]. Eif2s2 is also down in cachexia (Fig. 3K) This gene codes for a subunit of the eIF2 complex, and it is known that overexpression of this gene can induce muscle hypertrophy[31], and the decrease in cachexia could therefore be contributing to muscle loss and a decrease in protein synthesis. Two other genes in the top 20 DEGs that are upregulated in cachexia are Cebpd and MT1 (Fig. 3L,M). Cebpd is a transcription factor that has a function in inducing inflammatory gene expression[32]. This may be one of the causes of the increase in inflammatory cytokine expression in MuSCs in cachexia, including Ccl11 and Il6. In male MuSCs, among the top 20 most differentially expressed genes, there are many genes important for proper MuSC function. We see that there is a large increase in OSMR expression (Fig. 3N). OSMR has multiple roles in MuSCs, particularly it is known to promote MuSC quiescence[33], and it can also induce muscle atrophy[34]. Furthermore, Chrdl2 and Gadd45g are both increased in cachexia (Fig. 3O,P). Both of these genes have roles in maintaining MuSC quiescence. Chrdl2 is a known marker of quiescence[35,36] and Gadd45g is a stress growth arrest factor[37]. We also see an increase in STAT3 expression in cachexia (Fig. 3Q). STAT3 is a crucial transcription factor that has a plethora of functions in MuSCs, including self-renewal, proliferation and differentiation[38-40]. Inhibition of STAT3 has been shown to improve muscle regeneration in aging[41]. More broadly, when performing a GSEA analysis, we see that there is a lot of overlap between male and female MuSCs in the enrichment of key pathways. In both sexes, we see a trend in the upregulation of Kras Signaling and, importantly, the Epithelial Mesenchymal Transition pathway when comparing control vs cachexia MuSCs. Among the downregulated pathways, we see that Oxidative Phosphorylation and MTORC1 are enriched in both male and females (Fig. 3R-U).

We found that many of the genes that were altered due to cachexia, were also genes that were deregulated in aging and we wanted to determine whether there is a correlation between cachexia and aging. To confirm this, we compared the changes in the transcriptome of Control vs. Cachexia Male MuSCs to the changes in the transcriptome of Young vs. Aged Male MuSCs. The Young vs Aged data were retrieved from publicly available data (GSE171997). We see that there is a correlation between the effect of cachexia vs the effect of aging (Expanded View Fig. 4A,B). Specifically, we highlight here that both cachexia and aging cause a decrease in the expression of *Sparc* and *Col3a1*(Expanded View Fig. 4C,D), important genes for the assembly of the ECM of the MuSC niche. There is also a decrease in CCND1 (Expanded View Fig. 4E), which may indicate that the cachectic MuSCs have a delay in the entry into cycle. The inflammatory cytokine genes,

Ccl7 and *Ccl11*, are both highly upregulated in cachexia and aging (Expanded View Fig. 4F,G), which may be drivers of the increase in inflammation seen in both conditions. Lastly, Rnase4 is upregulated (Expanded View Fig. 4H), a gene that is involved in mRNA processing and could indicate changes to translation. Together, the data presented here demonstrates that cachexia induces large transcriptomic changes whose effects are multifaceted, affecting the ECM, inflammation, cell cycle and metabolism, among others.

Cachexia Alters Chromatin Accessibility in MuSCs

Cachexia greatly affected the transcriptome of the MuSCs and we wanted to determine whether chromatin accessibility was also affected, as that can act as a regulator of gene expression. Using freshly isolated MuSCs from 4-month-old healthy control or tumor bearing female mice, we performed an ATAC-Seq (Fig. 4A). We see that cachexia greatly alters the chromatin accessibility of MuSCs. At a threshold of adjusted p-value ≤ 0.05, there are 6715 significantly differentially accessible peaks (Fig. 4B). Additionally, we do see that on a PCA plot the control and cachectic MuSCs cluster separately (Fig. 4C). We associated the peaks with the nearest gene and performed a GSEA analysis. We see that many of the Hallmark pathways that are enriched in the ATAC-Seq samples are the same as the ones enriched in the RNA-Seq samples (Fig. 4D). For example, Kras Signaling, Inflammatory Response, Il6-Jak-Stat3 Signaling and the EMT pathways are all upregulated, as is the case with the RNA-Seq results. This would suggest that many of the transcriptomic changes seen in the MuSCs could be explained by alterations to chromatin accessibility and the chromatin state. Further supporting the effect of alterations in chromatin accessibility, we see that genes such as Myogenin and CCND1 have a decrease in accessibility in cachexia (Fig. 4E-G), while simultaneously having a decrease in mRNA expression. Both of these genes are important for MuSC function, with myogenin being necessary for differentiation and fusion into myofibers, while CCND1 promotes MuSC proliferation and expansion.

Lastly, we wanted to determine whether these changes in chromatin accessibility also led to changes in transcription factor binding. By analysing the DNA sequences under the differentially accessible peaks between control and cachexia MuSCs, we discovered that 88 transcription factors had a significant change in the number of binding motifs present in the peaks (Fig. 4H). Many of the transcription factors that show an increase in their number of motifs are part of the Jun and Fos transcription factor families (Fig. 4H,I). The upregulation of these transcription factors is associated with stress response and inflammation and has been determined to upregulate Fos expression[42]. Importantly, ATF4 has more accessible binding sites in cachexia than in healthy controls (Fig. 4J). ATF4 is a master regulator of the integrated stress response and the increase in accessibility of sites containing its motif could be a driver of the observed increase in expression of stress response genes in cachectic muscle stem cells. Interestingly, we see that every myogenic regulatory factor (MRF) has a decrease in the number of accessible binding sites in the cachexia condition (Fig. 4K-N). Myf5, MyoD, Myogenin and Myf6 are all essential for the myogenic program to properly unfold. The loss of binding sites for the myogenic regulatory factors could be a major cause for MuSC dysfunction in cachexia.

MuSCs Exhibit Functional Decline in Cachexia

To further elucidate whether MuSCs are functionally affected by cachexia, we isolated EDL myofibers and TA muscles from 4-month-old mice 2-3 weeks after C26 tumor cell injections. We found that EDL myofibers from cachectic mice had a significantly reduced number of MuSCs (Fig. 5A,B), and similarly, from the TA cross sections we see that there are also less MuSCs in cachexia

compared to healthy controls (Fig. 5C,D). Importantly, it appears that there is a large decrease in the expression of PAX7 in MuSCs from tumor bearing mice. PAX7 is essential for the maintenance of the MuSC pool and a large decrease in its expression could be the primary cause of the loss in MuSC number and function[43]. However, it is important to note that this decrease in PAX7 protein is not reflected in the transcriptome. From the RNA-Seq, there is no significant decrease in *Pax7* expression. Therefore, it is probable that this decrease in PAX7 protein is due to translational changes in cachexia.

To determine whether skeletal muscle regeneration was affected by C26 cancer, we injected 3-month-old mice with C26 cells. After 1 week of incubation, the TA of the mice were injured with cardiotoxin (CTX) and allowed to recover for 7 days. We see that the TAs of mice that had cancer did not regenerate as well as those from healthy controls (Fig. 5E). The regenerating fibers from cachexia are smaller and we see a large decrease in the number of MuSCs (Fig. 5F,G), which would further compromise the regenerative capacity of the muscle.

When MuSCs are removed from the tumor environment, they quickly recover. When we cultured isolated EDL myofibers for 48 hours, we found that the MuSCs were capable of expanding and nearly reach the levels of the controls (Fig. 5H,I). By 72 hours, the number of MuSCs in the cachexia condition was equal to those in the control (Fig. 5J,K). These results indicate that MuSC function is altered due to cancer driven changes in the niche environment.

To determine whether C26 cells directly affect MuSC function, we performed a trans-well assay where isolated EDL myofibers were cocultured with C26 cells. Being exposed to C26 cells greatly affected the ability of the MuSCs to activate and proliferate. At 48 hours of coculture, there was almost no increase in the number of MuSCs on the EDLs cultured with C26 cells (Fig. 5l). This trend continued after 72 hours of coculture with C26 cells, with a significant decrease in the number of MuSCs (Fig. 5M,N). The same results were seen when the myofibers were cultured in C26 conditioned media. After 72 hours, the number of MuSCs on the myofibers in the conditioned media was significantly less than the number in the normal growth media, with numbers similar to those cultured in unsupplemented growth media (Expanded View Fig. 5A,B). Interestingly, we also saw a significant decrease in the number of Myogenin positive MuSC in the conditioned media (Expanded View Fig. 5A,C). To see whether this could be replicated in primary myoblasts, we cultured primary myoblasts in C26 conditioned media for 12, 24, and 36 hours. At all time points we found that there was a significant decrease in the percentage of Myogenin expressing cells (Expanded View Fig. 5D-I). In Cell Western Blot of primary myoblasts confirmed that when cells are cultured in C26 conditioned media there is a significant reduction in Myogenin and a decrease in MyoD (Expanded View Fig. 5J-L). Myogenin is the MRF that is responsible for the fusion of myoblasts into myotubes[44], as such we wanted to determine whether this observed decrease in Myogenin would translate into deficient differentiation. An In Cell Western Blot of primary myotubes cultured for 3 days in C26 conditioned differentiation media revealed a significant decrease in MyHC expression (Expanded View Fig. 5L,M). We cultured primary myoblasts for 5 days in C26 conditioned differentiation media to assess the effect on Myogenin expression and the fusion of these cells. We found that the conditioned media resulted in a decrease in Myogenin positive nuclei, consistent with our findings in the primary myoblasts (Expanded View Fig. 5N,O). We also noted a decrease in the fusion of the cells into myotubes and a decrease in the size of the myotubes themselves (Expanded View Fig. 5P-Q). All together, the data presented here indicates that C26 cancer cells are capable of directly communicating with MuSCs. This

communication has a broad deleterious effect on the myogenic program, reducing expansion of the MuSC pool and impeding differentiation.

C26 Tumor Cells Adapt to the Host Environment

To further elucidate the communication network between C26 cells and MuSCs, we needed to assess the transcriptome of the C26 cells. We also wanted to determine whether the transcriptome of the C26 cells was altered when the cells were engrafted and grown *in vivo* compared to cultured *in vitro*, as well as whether the sex of the host mouse had any bearing. To achieve this goal, we created a GFP over expressing C26 cell line through retroviral infection. The GFP cells were injected into 3-month-old male and female Balb/c mice and allowed to form tumors (Fig. 6A). The tumors were grown until the mice neared endpoint. At that time the tumors were dissected and single cell suspensions created to FACS sort the GFP positive cells (Fig. 6B,C). RNA-Seq libraries were generated from the cultured *in vitro* GFP C26 cells, as well as the GFP C26 cells isolated from male and female mice.

From the sequencing results, we see that there is a large change in the transcriptome when the C26 cells were grown *in vivo*, with the *in vivo* samples clustering away from the *in vitro* ones (Fig. 6D,E). Interestingly, there are far more genes that are differentially expressed between the *in vitro* and *in vivo* samples than when comparing male and female grown cells. At a threshold of adjusted p-value ≤ 0.1, there are 7880 upregulated and 3155 downregulated genes between *in vitro* and *in vivo* in females, while only having 200 upregulated and 272 downregulated genes between female and male *in vivo* C26 cells (Expanded View Fig. 6A). The results are even more striking when using our most stringent threshold of adjusted p-value ≤ 0.001. Between *in vitro* and *in vivo* in females there are 4708 and 907 upregulated and downregulated genes, respectively. However, between *in vivo* female and male, there is a paltry 11 genes that are significantly upregulated and 20 that are significantly downregulated (Expanded View Fig. 6A). The sex of the host appeared to have a minimal effect on the transcriptome of the C26 cells, when compared to the effect seen between *in vitro* and *in vivo* (Fig. 6F-I; Expanded View Fig. 6B,C). From the GSEA analysis, we see that there is a large overlap in the enriched Hallmark pathways when comparing *in vitro* vs *in vivo* in female and *in vitro* vs *in vivo* in male. Among the top enriched pathways, Allograft Rejection, Complement, Kras Signaling, and Il6 Jak Stat3 Signaling are upregulated in both comparisons (Fig. 6J; Expanded View Fig. 6D). We also see that Inflammatory Response, EMT and Il6 Jak Stat3 Signaling pathways are enriched when comparing *in vivo* in female vs *in vivo* in male (Fig. 6K). Together, these data indicate that C26 cells adapt to the *in vivo* environment to promote their survival and growth, but that the sex of the host has no major effect on C26 behaviour.

Our results indicate that many immune cell genes are upregulated in the *in vivo* condition compared to the *in vitro*. To ensure that the changes in the transcriptome previously observed were not due simply to host cell contamination or our RNA-Seq, we further assessed the expression of immune related genes. We found that while there was an upregulation of many immune genes *in vivo*, including *Adgre1* and *Mrc1*, many immune genes were not expressed at all, such as *CD163* and *MARCO* (Expanded View Fig. 6E). This makes it unlikely that there is immune cell contamination as there would not be selective expression of certain immune related genes, but rather an increase in all the immune genes. Interestingly, some immune genes were already expressed in the *in vitro* cultured condition, in which there could not be any immune cell contamination, including CD14 and CD80 (Expanded View Fig. 6E). To further confirm there are no host contaminating cells in the samples, we analyzed the expression of Y chromosome genes. We chose to do this because

C26 cells were originally derived from female Balb/c mice and are therefore female cells lacking a Y chromosome. If there were to be contamination from the host, we would see expression of Y chromosome genes in the *in vivo* in male mice condition. However, that is not the case, there is no upregulation of Y chromosome genes in the *in vivo* in male condition compared to *in vitro* and *in vivo* in female (Expanded View Fig. 6F,G). Using our male and female MuSC RNA-Seq data for comparison, we see that only the male MuSCs express Y chromosome genes, with the C26 cells resembling the female MuSCs (Expanded View Fig. 6F). These results indicate that there is no contamination from other cell types, and that it is the C26 cells that are expressing these immune genes. We speculate that the C26 cells are undergoing immune mimicry to evade the host immune system.

Cancer Increases Circulating MMP9 and GDF15 Which Impedes MuSC Function

C26 tumors are solid tumors that we have injected subcutaneously and therefore are not present in the muscle itself. Any communication that C26 cells have with muscle cells must therefore be through the production of signaling molecules that travel through the blood. To assess how the cytokine landscape is altered in cachexia, we performed a Cytokine Array on serum from male and female mice that were either healthy or injected with C26 tumors. Several cytokines changed their levels due to cachexia, with a particular interest in MMP9 and GDF15 (Fig. 7A,B). From the array, we see that in cachexia MMP9 levels are approximately 5 times and 3 times higher in male and female mice, respectively (Expanded View Fig. 7A,B). Similarly, GDF15 is approximately 25 times higher in cachectic male mice compared to controls, and approximately 4 times higher in cachectic females (Fig. 7C,D). These cytokines are produced by the C26 cells, with MMP9 being expressed only in the C26 cells, not in MuSCs or Myofibers, and increasing in transcriptional expression when C26 is grown *in vivo* (Expanded View Fig. 7C). GDF15 is produced in both the C26 cells and MuSCs, with its expression transcriptionally decreasing when C26 cells are grown *in vivo* (Fig. 7E,F).

From the cancer genome atlas (TCGA) we retrieved human data from patients with colon adenocarcinoma and pancreatic adenocarcinoma. Only patients that did not receive chemotherapy or surgery were selected. From these data, we see in both types of cancer that the patients that had higher levels of GDF15 or MMP9 had a worse prognosis than those that had lower levels of the cytokines (Expanded View Fig. 7D-G). These findings highlight the potential role of GDF15 and MMP9 in cancer progression.

Both GDF15 and MMP9 are known to induce the expression of SNAI1 and upregulate the EMT pathway. This is of particular interest as we see from the RNA-Seq data that the EMT pathway is upregulated in cachectic MuSCs, and specifically we see a large upregulation of *Snai1* expression (Fig. 7G). We confirm with qPCR that primary myoblasts cultured in C26 conditioned media have an increase in *Snai1* transcript (Expanded View Fig. 8A), indicating that it is through direct signaling between cancer cells and myogenic cells that induces the upregulation of Snai1. Previous studies have shown that SNAI1 represses myogenic differentiation by outcompeting MyoD binding and blocking the expression of Myogenin[45]. An aberrant over expression of SNAI1 can block the ability of myogenic cells from differentiating and fusing into myotubes. These findings are corroborated by our MuSC RNA-Seq data, where we see a decrease in Myogenin expression and key differentiation genes, such as *Mymk*, which is necessary for myoblast fusion (Fig. 7H,I).

To determine whether MMP9 can directly induce SNAI1 expression in primary myoblasts, we treated these cells with MMP9 for 12 hours. Staining revealed that there was a higher percentage

of High SNAI1 expressing cells in the MMP9 treated condition compared to the controls (Expanded View Fig. 8B,C). However, we did not observe a decrease in Myogenin at this timepoint (Expanded View Fig. 8C,D). Further, we treated EDL myofibers, that were cultured 36 hours prior, with MMP9 for 1 hour and then stained for phosphor-SMAD3 (Expanded View Fig. 8D). Exposure to MMP9 resulted in an increase in phosphor-SMAD3 staining compared to controls (Expanded View Fig. 8E). These results suggest that MMP9 can directly signal to myogenic cells and induce the expression of SNAI1.

We also wanted to determine whether GDF15 can directly signal to MuSCs. Freshly isolated EDL myofibers were cultured in unsupplemented growth media and treated with GDF15. 24 hours post isolation, we see that while there was no change in the MuSC number, there is an increase in the percentage of High SNAI1 expressing MuSCs (Fig. 7J-L). However, at 60 and 72 hours of culture, we see that compared to the unsupplemented myofibers, the GDF15 treatment resulted in an increase in MuSC number and a decrease in Myogenin expressing MuSCs (Fig. 7M,N; Expanded View Fig. 8F-H). Primary myoblasts were then treated for 24 hours with GDF15, and similar results were obtained. Primary myoblasts that were treated with GDF15 had higher levels of SNA1 and lower levels of Myogenin compared to the unsupplemented condition (Expanded Fig. 7P-R). Together, these data indicate that MMP9 and GDF15 can affect MuSC function, promoting proliferation at the expense of differentiation.

Blocking Snai1 Rescues Defect in Differentiation and Prevents Cell Death

It has previously been established that SNAI1 is a potent inhibitor of myogenic differentiation[45]. We questioned whether reducing SNAI1 via siRNA knockdown would restore the differentiation potential of primary myoblasts exposed to C26 conditioned media. Cells were treated with siSNAI1 or siControl and then differentiated for 3 days in either normal differentiation media or C26 conditioned differentiation media. We found that the knockdown of SNAI1 resulted in an increase in fusion even in the normal differentiation media, increasing from approximately 40% fusion in the siControl condition to 60% (Fig. 7O-P). Importantly, the knockdown of SNAI1 was able to partially rescue the defect in differentiation when cells are cultured in conditioned media. The siControl cells only had a fusion index of approximately 20% while the SiSNAI1 treated cells had a fusion index of approximately 35% (Fig. 7Q,R). Furthermore, there is a restoration of Myogenin levels in the siSNAI1 condition, however not to the levels of cells that are cultured in normal differentiation media. (Fig. 7S,T).

When myoblasts are differentiated in C26 conditioned media, we observed a large number of floating cells and a decrease in the number of cells, indicating that these cells were undergoing cell death. We determined that these cells were lost from apoptosis as evidenced by the high percentage of cells, approximately 80%, expressing Cleaved Caspase3 (Fig. 7S,U). The knockdown of SNAI1 was able to partially rescue the cell death phenotype with only approximately 25% of cells being cleaved Caspase3 positive (Fig. 7S,U). Together these results highlight the role of SNAI1 upregulation in the defect of the MuSC pool and differentiation potential in cachectic mice.

Knockout of GDF15 in C26 Cells does not Prevent Cachexia

GDF15 has recently become a protein of great interest in the field of cachexia research. Recent studies have shown that GDF15 can suppress the appetite of cancer patients and that, by blocking GDF15 in the body, cachexia can be prevented[46]. We wanted to determine whether knocking out GDF15 in C26 tumors can prevent muscle wasting in mice. To achieve this, we generated Crispr

GDF15 knockout and Crispr Control C26 cells. Mice were subcutaneously injected with the Crispr cells and tumors were allowed to grow until mice reached endpoint. Surprisingly, the GDF15 KO tumors grew faster, and mice reached endpoint within 3 weeks, compared to Crispr Control tumors where mice who reached endpoint between 4-5 weeks post tumor injection. However, this does not appear to be due to differences in proliferation between the cells as *in vitro* EDU assays showed equal EDU incorporation (Expanded View Fig. 9A,B) The KO of GDF15 in the C26 cells had no effect on body mass, with both the KO and the controls losing the same amount of body weight (Expanded View Fig. 9C). The GDF15 KO tumors grew larger than the controls (Expanded View Fig. 9D) and interestingly, the TA muscle mass was significantly reduced in the GDF15 KO tumor condition compared to the Crispr Control mice (Expanded View Fig. 9E). The TA cross sectional area of the GDF15 KO tumor mice was slightly reduced compared to the Crispr controls as well (Expanded View Fig. 9F,G). Overall, there was no significant difference between the percentage of fat mass and lean mass between the Crispr Control and GDF15 KO tumor bearing mice (Expanded View Fig. 9H,I). We also validated the levels of circulating GDF15 and found that while there was a significant reduction of GDF15 in the serum of the Crispr KO tumor bearing mice, there was still GDF15 present, meaning that the tumor is not the sole source of GDF15 in the body (Expanded View Fig. 9J). Furthermore, the KO of GDF15 in the tumor did not result in any differences in metabolism or food consumption during the second week post tumor injection (Expanded View Fig. 9K,L). We do see, surprisingly, that there was a trend towards a lower daily food intake in the GDF15 KO tumor bearing mice (Expanded View Fig. 9M). This is contrary to expectations as GDF15 is a known appetite suppressor. However, as previously stated, the GDF15 KO tumors grew faster and at this time point the mice in the GDF15 KO cohort were nearing endpoint, while the Crispr Controls were still relatively healthy. This could explain the discrepancy. We also observed a trend of the GDF15 KO tumor bearing mice shifting their energy consumption towards fat instead of carbohydrates, as evidenced by the decrease in RER towards 0.7 (Expanded View Fig. 9N).

Next, we assessed the effect of knocking out GDF15 in the C26 tumors on MuSC numbers. Freshly isolated EDL myofibers were stained for Pax7 and the MuSC number quantified. We found that there was no difference between the Crispr Control and GDF15 KO conditions, both exhibited a similar reduction in MuSC number when compared to healthy controls (Fig. 8A,B). We also quantified the number of MuSCs in TA cross sections, and the same result was obtained, both tumor conditions resulted in an equal loss of MuSCs (Fig. 8C,D). We then assessed how primary myoblasts cocultured with GDF15 KO C26 cells were affected. We found that there was no change in the proliferation of primary myoblasts, as evidenced by EDU incorporation (Expanded View Fig. 10A,B). Further, differentiation was equally reduced when cells were differentiated in the presence of Crispr Control or GDF15 KO C26 cells (Expanded View Fig. 10C,D). We did observe, however, an increase in the number of MuSCs in the EDL myofibers that were cocultured with the GDF15 KO C26 cells when compared to those cultured with the Crispr Control cells, as well as a reduction in Myogenin positive MuSCs (Expanded View Fig. 10E-F). As a whole the data presented here indicates that, in mice, the knockout of GDF15 in the tumor is not sufficient to rescue the cachexia phenotype and does not prevent the loss of MuSCs.

Pharmacological Inhibition of MMP9 Restores MuSC Pool in Cachectic Mice

MMP9 is known to induce SNAI1 expression in cancer cells[47]. The drug JNJ0966 is an MMP9 zymogen inhibitor[48]. It functions by preventing the proprotein MMP9 from being cleaved into its active form. It is highly specific and does not block the activation of proMMP1, 2 and 3[48]. We

wanted to determine whether the pharmacological inhibition of MMP9 can rescue the cachectic phenotype.

Mice were injected with C26 cells and the tumors were allowed to grow for 7 days. On Day 7, the mice were injured with BaCl2 injection in the TA muscle and then given daily JNJ0966 or DMSO subcutaneous injections. Mice treated with the MMP9 inhibitor did not lose as much body weight as their control counterparts, despite having the same tumor sizes (Fig. 8E.F). The TA muscles from the uninjured leg were significantly larger relative to the total body weight in the JNJ0966 treated mice compared to the DMSO controls (Fig. 8G). A similar trend was observed in the injured TAs but did not reach statistical significance (Fig. 8H). However, there was no significant change in the CSA of the TA myofibers in either injured or uninjured TA muscle (Fig. 8I-K).

Our findings show that cachectic mice exhibit a decline in the MuSC pool. We quantified the number of MuSCs on EDL myofibers freshly isolated from tumor bearing mice treated with JNJ0966 or DMSO. We found that the mice that had MMP9 inhibited had a significantly higher number of MuSCs per EDL myofiber, averaging approximately 6 MuSCs per fiber in contrast with the average 4 MuSCs per myofiber in the DMSO control (Fig. 8L,M). In addition, we see the same results in the TA cross sections. In the uninjured TAs there is a significant increase in the MuSC pool of the JNJ0966 treated mice, averaging at 10.45 MuSCs/mm^2, compared to the 3.65 MuSCs/mm^2 in the DMSO control (Fig. 8N,O). The increase in the MuSC pool is even more striking in the injured TA muscle. Earlier, we found that cachectic mice fail to expand their MuSC pool when the muscle is injured (Fig. 5G). The JNJ0966 treatment rescues that defect and shows an expansion of the MuSC number in response to injury, with an average of 52.7 MuSCs/mm^2, while the DMSO control mice only possessed an average of 5.21 MuSCs/mm^2 (Fig. 8N,O).

These data together indicate that MMP9 is a potential target as novel cancer cachexia therapy. By inhibiting MMP9 activation we were able to restore the MuSC pool in cachectic mice and reduce the loss of body weight.

DISCUSSION

Cancer cachexia induces extensive remodeling of skeletal muscle that extends beyond mature myofibers to the resident muscle stem cell compartment. Using an integrated approach combining single-myofiber and MuSC RNA-seq, ATAC-seq, proteomic tracing, and regeneration assays, we show that cachexia is associated with broad suppression of the myogenic differentiation program together with metabolic and stress-associated remodeling. Our findings further support a model in which tumor-derived secreted factors contribute to a reversible disruption of MuSC function, with induction of EMT-like phenotype as mediator of impaired muscle stem cell differentiation in cachectic condition.

Single-myofiber RNA-seq shows that cachexia drives extensive transcriptional alterations leading to significant changes in their genetic network related to metabolic state and stress response. The upregulation of PDK4, ACOT1, and ACOT2 suggests a shift toward fatty-acid oxidation, consistent with decreased respiratory exchange ratio and fat mass observed *in vivo* (Fig. 2). Additionally, downregulation of Mafa, Myh4, and Ampd1 suggest selective susceptibility of fast-twitch fibers to cachexic environment (Fig. 2). Enrichment of hypoxia and apoptotic pathways, coupled with repression of WNT and Notch signaling, highlights a reduction of anabolic programs within the myofibers. These alterations are in line with human cachexia studies implicating

oxidative stress, mitochondrial dysfunction, and metabolic reprogramming as important drivers of atrophy[49-52].

In the cachectic environment MuSCs exhibit reduced expression of extracellular-matrix and niche-organizing factors such as Col3a1 and Sparc, respectively and key regulators of proliferation and translation (CCND1, Eif2s2), alongside induction of inflammatory and quiescence-associated transcripts (Ccl7, Il6, Osmr, Chrdl2, Stat3) (Fig. 3). Pathway enrichment analysis implicates EMT, IL6–JAK–STAT3, and KRAS signaling, and suppression of oxidative phosphorylation and mTORC1 activity for muscle stem cells. These data collectively suggest a chronic stress-induced, regeneration deficient state. Interestingly, comparison of gene expression data with aged MuSCs reveals a substantially common transcriptomic signature between cachectic and aged muscle stem cells, suggesting that cachexia phenocopies aspects of muscle stem cell aging through activation of inflammatory pathways and metabolic reprogramming (Expanded View Fig. 4).

ATAC-seq provides further mechanistic insight into this reprogramming. In freshly sorted muscle stem cells, cachexia reduces chromatin accessibility at the Myogenin and CCND1 loci while enhancing the accessibility of ATF4, FOS and JUN binding motifs. These findings suggest that stress-responsive factors dominate the cachectic regulatory landscape, concurrent with the repression of the myogenic differentiation network. Such differentiation related chromatin erosion mirrors observations in aging and dystrophic contexts where environmental stress remodels stem-cell epigenomes[53-55]. Although MuSCs from cachectic mice display impaired proliferation and regenerative capacity, they rapidly regain their function *ex vivo*, underscoring that their dysfunction is largely reversible and niche-driven rather than due to cell-intrinsic dysregulation (Fig. 5).

Transcriptomic profiling of GFP-labeled C26 cells before and after injection into the mice revealed a dramatic *in vivo* reprogramming, including activation of IL6–JAK–STAT3, KRAS, and EMT pathways, as well as induction of Adgre1 and Mrc1. These changes were independent of host sex, suggesting that tumor adaptation to the host microenvironment rather than hormonal milieu drives cachexia-relevant signaling. The upregulation of immune-associated transcripts in tumor cells, without host cell contamination, suggests that C26 cells acquire immune cell-like features, likely with the purpose to evade immune surveillance while simultaneously secreting cytokines that affect peripheral tissues.

Serum profiling from mice using cytokine array identified GDF15 and MMP9 as tumor-derived factors that were highly elevated during cachexia (Fig. 7). GDF15, a TGFβ superfamily cytokine, has been implicated in appetite suppression and systemic energy imbalance[56,57] and has been implicated in the induction of SNAI1[58]. On the other hand, MMP9 is known as an ECM-remodeling protease, which plays an important role in ECM remodeling and controls cell adhesion and polarity[59,60]. MMP9 is also implicated in activation of latent TGFβ ligands[61], and is shown to promote SNAI1 induction via SMAD3 phosphorylation[47].

The upregulation of SNAI1 has been previously implicated in blocking differentiation of myoblasts into myotubes[45]. We found that MuSCs from cachectic mice and myoblasts exposed to C26 cells had an increase in SNAI1 expression and failed to differentiate. By knocking down SNAI1 we were able to rescue the defect in differentiation and prevent cell death in myoblasts cultured in C26 conditioned media. These findings highlight SNAI1 and the upregulation of the EMT pathway as key drivers of the decline in MuSC function and number in cachectic mice.

Although upregulation of Snai1 in muscle stem cells from cachectic mice and their impaired differentiation correlates with upregulation of tumor-derived GDF15 and MMP9, we cannot establish a direct relationship between Snai1 induction in muscle cells and GDF15/MMP9 from tumor cells with our current data. Interestingly, knockout of GDF15 in C26 tumors did not rescue muscle wasting, revealing redundancy from host or stromal sources such as macrophages and myofibers themselves (Fig. 8).

While the removal of tumor derived GDF15 did not result in any improvement in muscle wasting, we determined that pharmacological inhibition of MMP9 using the drug JNJ0966 does lead to an improvement. We see that mice treated with JNJ0966 have a reduced loss of body weight due to the cancer and are able to maintain their MuSC pool and even expand it in the case of injury (Fig. 8). A previous study found that MMP9 derived from gastric cancer associated macrophages induces metastasis through activation of the PI3K/AKT/SNAI1 pathway and by inhibiting MMP9 with JNJ0966 metastasis was blocked[47]. These results implicate MMP9 inhibition as a potential therapeutic target in cancer cachexia.

Together, our findings support a model in which C26 tumor cells undergo substantial transcriptional adaptation within the host and generate a circulating signaling environment that alters skeletal muscle and its resident stem cells. In MuSCs, this environment is associated with metabolic and stress-response remodeling, reduced accessibility of the myogenic regulatory landscape, and induction of a SNAI1-associated EMT-like transcriptional program that suppresses differentiation and promotes cell death (Fig. 9). GDF15 contributes to this signaling landscape but is not by itself required for the cachectic phenotype, whereas MMP9 emerges as a potential candidate upstream regulator whose pharmacological inhibition preserves the MuSC pool and restores its capacity to expand after injury. Thus, rather than establishing a single-factor pathway, our data define a combinatorial framework in which tumor-derived and host-derived signals converge on reversible cell-state changes in MuSCs, identifying SNAI1-associated myogenic suppression and MMP9 activity as potential points of therapeutic intervention in cancer-associated regenerative failure.

Materials

Reagent or Resource	**Source**	**Identifier**
Antibodies		
PAX7	DSHB	RRID: AB_528428
MYOD1 (G1)	Santa Cruz	Cat# Sc-377460; RRID: AB_2813894
Myogenin	DSHB	RRID: AB_2146602
MF20	DSHB	RRID: AB_2147781
SNAI1	Novus Biologicals	Cat# NBP2-27184; RRID: AB_2797904
Phosphor-SMAD3 (S423/425)	Cell Signaling	Cat# 9520S; RRID: AB_2193207
Anti-mouse ITGA7-Alexa647	R&D Systems	Cat# FAB3518R; RRID: AB_10973483
Anti-mouse PE-CD11b	Invitrogen	Cat# 12-0112-82; RRID: AB_2734869
Anti-mouse PE-CD31	BD Pharmigen	Cat# 553373; RRID: AB394819

Anit-mouse PE-Sca1/Ly6A-E	BD Pharmigen	Cat# 553108; RRID: AB_394819
Anti-mouse PE-CD45	Invitrogen	Cat# 12-0451-82; RRID: AB_465668
Alexa Fluor 488 goat anti-rabbit IgG	Invitrogen	A11008
Alexa Fluor 594 goat anti-mouse IgG2b	Invitrogen	A21145
Alexa Fluor 594 goat anti-rabbit IgG	Invitrogen	A11012
Alexa Fluor 488 goat anti-mouse IgG1	Invitrogen	A21121
Alexa Fluor 594 goat anti-mouse IgG1	Invitrogen	A21125
Alexa Fluor 647 goat anti-rabbit IgG	Invitrogen	A21245
Chemicals and Recombinant Proteins		
Fetal Bovine Serum	Wisent	080-450
10% Goat Serum	Thermofisher	50062Z
Horse Serum	Wisent	065-150
BSA	Sigma Aldrich	9048-46-8
Glycine	Bioshop	GLN001.5
Sucrose	Millipore Sigma	S7903
Triton-X100	BioShop	TRX777.500
Ham's F10 Nutrient Mix	Thermofisher	11550043
DMEM	Thermofisher	11965118
RPMI 1640	Thermofisher	11875093
PBS 1X	Wisent	311-013-CL
Penicillin-Streptomycin (10,000 U/mL)	Thermofisher	15140122
bFGF	Thermofisher	PHG0266
Collagen from rat tail tendon	Millipore Sigma	11179179001
2-Methylbutane	Millipore Sigma	270342
Frozen Section Compound	VWR	95057-838
Collagenase D	Millipore Sigma	1108888201
Dispase II	Millipore Sigma	4942078001
Hoechst	Thermofisher	62249
Paraformaldehyde	Electron Microscopy Sciences	15714
Prolong Gold Antifade Mountant with DNA Stain DAPI	Thermofisher	P36931
Ampure XP beads	Beckman Coulter	A63882
Cardiotoxin	Latoxan	L8102-1MG
L-Lysine-2HCl, 13C6, 15N2	Thermofisher	88432

L-Arginine-$^{13}C_6$,$^{15}N_4$ hydrochloride	Millipore Sigma	608033
Recombinant Mouse GDF-15 (CHO-expressed) Protein	R&D Systems	10596-GD-025
Recombinant Mouse MMP-9 Protein	R&D Systems	909-MM-010
JNJ0966	R&D Systems	6439
Commercial Kits		
Click-iT EdU Cell Proliferation Kit for Imaging Alexa Fluor 594 Dye	Thermofisher	C10339
SMART-Seq HT Kit	Takara Bio	634456
Nextera XT DNA Library Preparation Kit	Illumina	FC-131-1024
Nextera XT Index Kit	Illumina	FC-131-1001
Tagment DNA Enzyme and Buffer (Small Kit)	Illumina	20034210
Proteome Profiler Mouse XL Cytokine Array	R&D System	ARY028

Methods

Mouse Strains and Animal Care

All mouse procedures conducted in this study were approved and performed in accordance with the guidelines set by the University of Ottawa's Animal Care and Veterinary Services (ACVS) committee. Male and Female Balb/c mice were used in this study. All the mice used in the experiments are age and sex matched. All the mice that were used in experiments were 4 weeks old and 3-4 months old. Mice were maintained at 21°C with 20% humidity under a 14-hour light/10-hour dark cycle, food and water were provided *ad libitum*.

Cell Culture

C26 adenocarcinoma cells were cultured with growth media (RPMI supplemented with 10% FBS, 1% penicillin/streptomycin) in an incubator at 37°C and 5% CO_2. Cells were passaged at 70% confluency.

Primary myoblasts were cultured on collagen (Roche, 11179179001) coated plates with growth media (Ham's F10 (Gibco, 11550043) supplemented with 20% FBS, 1% penicillin/streptomycin and 5 ng/mL of bFGF (Thermo Fisher, PHG2066)) in an incubator at 37°C and 5% CO_2. Cells were passaged at 70% confluency. For conditioned media experiments, conditioned media was created by culturing C26 in primary myoblast growth media for 48 hours. The media was collected and centrifuged at 500 g to remove residual cells. Myoblasts are cultured in with conditioned media at a 1:1 ratio with normal differentiation media.

Primary Myoblast Differentiation

Cultured myoblasts were grown to 90% confluence and differentiated in DMEM supplemented with 5% horse serum (HS) and 1% penicillin/streptomycin for the duration of the experiment. After

3 days the media was replaced with fresh differentiation media for the duration of the assay. For conditioned media experiments, conditioned media was created by culturing C26 in differentiation media for 48 hours. The media was collected and centrifuged at 500 g to remove residual cells. Myoblasts are cultured in with conditioned media at a 1:1 ratio with normal differentiation media.

C26 Tumor Injection

Cultured C26 cells were trypsinized and the number of cells counted using Trypan Blue. The cells were suspended in 2% FBS/PBS. Mice were anesthetized with isoflurane and were injected twice, subcutaneously, with 1 million C26 cells each injection. Tumors were allowed to grow until the mice reached endpoint, or until the end of the experiment. Mice injected with Crispr C26 cells were given two injections of 2 million cells each.

Generation of GFP C26 Adenocarcinoma Cells

Stable cell lines of C26 GFP expressing cells were generated as previously described[62]. Briefly, retrovirus particles containing the eGFP Plasmid were generated in Phoenix helper-free retrovirus producer lines using lipofectamine transfection. The viral supernatant was collected 48 h after transfection and subsequently applied to cultured C26 cells for 8 h. The cells were then washed twice with 1 × PBS and grown for 48 h in normal growth media. Cells were cultured in Puromycin Selection Media (DMEM supplemented with 10% FBS, 1% penicillin/streptomycin, and 2.5 μg/ml puromycin) for 1 week. The cells were then cultured in Low Puromycin Maintenance Media (DMEM supplemented with 10% FBS, 1% penicillin/streptomycin, and 1.25 μg/ml puromycin).

Generation of GDF15 Crispr KO C26 Cells

CRISPR guide RNAs targeting exon 1 of Gdf15, this exon being common to all annotated isoforms, were designed[63] and cloned into pLentiCRISPRv2_GFP[64], such that guides did not share any potential off-target sequences. A control guide targeting Renilla luciferase was also cloned into the same vector. Guide sequences are given in Table 1. Lentiviral particles were generated from these vectors as previously described[65] and were used to transduce C26 cells. Transduced cells expressing GFP were sorted using a Sony SH800 Cell Sorter. Seven days post-transduction, genomic DNA was isolated from sorted cells and was used as template in a PCR reaction with primer pair GCGATTGCGTCAGATTTCCG & CCGAATTAGCCTGGTCACCC. PCR products were purified and subjected to sequencing using Oxford Nanopore technology (Plasmidsaurus, OR) with data being analyzed for gene disruption efficiency using Crispresso2 software[66]. The populations generated with the most efficient guides (2 and 3) as well as the control population were again sorted using a Sony SH800 but this time to single cells to generate monoclonal populations. Genomic DNA from these populations was then isolated and used as template in PCR reactions with the same primer pair as before, with the PCR products being subjected to Sanger sequencing. Sanger reads were de-convolved using the Tide software suite[67] to identify clones where out-of-frame knockout mutations had been introduced at the target site.

JNJ0966 Treatment

Mice were injected with C26 cells as described above. The tumors were allowed to grow for 7 days and then the mice tibialis anterior were injured with a 50 μL intramuscular injection of 1.2% $BaCl_2$. After injury, the mice were subcutaneously injected daily with 12mg/kg of JNJ0966 or with DMSO as a vehicle control, for 7 days.

Isolation of MuSCs by FACS

Muscle stem cells were isolated by Fluorescence Activated Cell Sorting (FACS) as previously described[55]. In brief, hindlimb muscles of the mice were dissected and mechanically minced. The minced muscles were transferred to a 15 mL conical tube and 5 mL of digestion buffer (F10 media, 10 U/mL Dispase II (Roche, 39307800), 2.4 U/mL Collagenase D (Roche, 11088882001) and 0.5mM $CaCl_2$). Muscles were initially digested on a shaker for 20 minutes at 37 °C and 5% CO_2. After the first round of digestion, the muscles were centrifuged for 10 seconds at 500g, and the supernatant was transferred to a fresh 50 mL conical tube containing 8 mL of FBS. The remaining muscle pellet was triturated and digested for a second time in an additional 5 mL of digestion buffer for 20 minutes. After the second digestion, the digested muscles were added to the same 50 mL conical tube containing the first digestion, and the entire mixture was filtered using a 40 µm cell strainer into a fresh 50 mL conical tube.

The filtered sample was centrifuged at 500g for 10 minutes at 4ºC. The supernatant was removed and the pellet resuspended in 500 µL of FACS Buffer (2% FBS and 0.5mM EDTA in PBS) containing the antibody mixture (Alexa 647- ITGA7 (1:500) (R&D systems, FAB3518R, clone # 334908) , PE-Cyanine7- VCAM-1 (1:500) (Invitrogen, 25-1061-82, clone # 429) ,PE-CD31(1:5000) (Invitrogen, 12-0311-82, clone # 390), PE-CD45 (1:5000) (Invitrogen, 12-0451-82, clone # 30F11), PE-CD11b (1:5000) (Invitrogen, 12-0112-82, clone # M1/70), PE-SCA1 (1:5000) (BD Biosciences, 553108, clone # D7) and Hoechst 33342 (Molecular Probes, H1399)). The samples were incubated for 20 minutes at RT with constant agitation and protected from light.

The samples were washed by adding 10 mL of FACS Buffer directly to the sample and centrifuging at 500g for 10 minutes. The supernatant was removed, and the cell pellet resuspended in 1 mL of FACS buffer. The samples were then filtered through a 40-µm cell strainer into a FACS compatible polypropylene round-bottom tube. The cells were sorted for the $ITGA7^+/VCAM1^+/Hoechst^+/CD31^-/CD45^-/CD11b^-/SCA1^-$ population as described previously with a Sony SH800 Cell Sorter[55].

FACS Sorting C26 Cells from Whole Tumor

Mice that were injected with GFP C26 tumor cells were euthanized and the whole tumor dissected. The whole tumor was mechanically minced and digested in 5 mL of digestion buffer (F10 media, 10 U/mL Dispase II (Roche, 39307800), 2.4 U/mL Collagenase D (Roche, 11088882001) and 0.5mM $CaCl_2$) for 15 minutes on a shaker at 37ºC and 5% CO_2. After, the digestion mix was centrifuged for 10 seconds at 500g and the supernatant transferred to a 50 mL conical tube containing 8 mL of FBS. The remaining tissue was triturated and another 5 mL of digestion buffer was added. The tissue was digested for 15 minutes on a shaker at 37ºC and 5% CO_2. The second digestion mixture was added to the 50 mL conical tube containing the first digestion and the sample was filtered using a 40 µm cell strainer into a fresh 50 mL conical tube. The sample was centrifuged at 500g for 10 minutes at 4ºC. The cell pellet was resuspended in 1mL FACS Buffer (2% FBS and 0.5mM EDTA in PBS) containing DAPI and filtered through a 40 µm cell strainer into a 5 mL round bottom polypropylene tube. The GFP C26 cells were sorted for the GFP+/DAPI- population using a Sony SH800 Cell Sorter.

Immunofluorescent Analysis of Cultured Cells

Cell culture media was removed, and cells were washed three times with PBS for 5 minutes at RT on a shaker. Cells were then fixed with 3.2% paraformaldehyde (PFA) (Electron Microscopy Sciences, 15714) in PBS for 5 minutes at RT and then washed three times in 1X PBS for 5 minutes. Cells were permeabilized for 15 minutes in 0.5% Triton-X and washed three times in 1X PBS for 5 minutes. Subsequently, cells were blocked in blocking buffer (0.1 M Glycine, 0.5% Bovine Serum Albumin (BSA) (Sigma, A8022), 0.3% Triton X-100 in PBS) for one hour at RT. Cells were incubated with primary antibodies diluted in the blocking buffer over night at 4 °C. The next day, the primary antibody solution was removed, and cells were washed three times with 0.1% Triton X-100 in PBS. After the washing step, secondary antibodies were diluted 1:400 in the blocking buffer and added to the cells for 1 hour at RT protected from light. Cells were washed three times with 0.1% Triton X-100 in PBS. Cells were mounted in mounting solution with DAPI and visualized under a microscope.

In Cell Western Blotting

Primary myoblasts were seeded onto collagen coated 96 well plates. Cells were fixed in 3.2% PFA and washed three times in PBS 1X. Cells were permeabilized with 0.5% Triton-X for 15 minutes and then washed three times in PBS 1X. Cells were blocked with blocking buffer (0.1 M Glycine, 0.5% Bovine Serum Albumin (BSA) (Sigma, A8022), 0.3% Triton-X in PBS) for 1 hour. Primary antibodies were diluted in blocking buffer, and the cells were incubated with the primary antibodies overnight at 4ºC. The primary antibody solution is removed, and the cells are washed three times with 0.1% Triton-X. Secondary antibodies were diluted 1:800 in the blocking buffer and added to the cells for 1 hour at RT protected from light. Cells were washed three times with 0.1% Triton X-100 in PBS. Cells were visualized using the Licor Odyssey M.

SiRNA Treatment

Cells underwent SiRNA treatment using the Lipofectamine RNAiMAX Reagent protocol. Briefly, primary myoblasts were cultured in 6cm plates to 80% confluency. Normal growth media was removed and replaced with 1.5mL antibiotic free growth media. RNA-Lipid complexes were formed by adding 750 uL of OPTI-MEM per 6cm plates to two tubes. In the first tube, 17 uL of Lipofectamine per 6cm plate was added. To the second tube, 100 pmol of siSNAI1 or siControl is added. The contents of both tubes are combined and thoroughly mixed. The solution is incubated at RT for 15 minutes and then 1.5mL of the solution is added in a dropwise fashion to thee 6cm plates. Primary myoblasts were cultured for 12 hours in the transfection media before replacing the media with differentiation media for 3 days.

Isolation and Culture of EDL Myofibers

Mice were sacrificed and the skin from the hindlimb was removed. The TA muscle was dissected out to expose the EDL muscle. The EDL was dissected by cutting the distal tendon and then the proximal tendon. The whole EDL was placed in an Eppendorf tube containing 800 µL of pre-heated (37 °C) myofiber digestion buffer (1000 U/ mL Collagenase (Sigma Aldrich, C0130) in unsupplemented DMEM). The EDL was placed in a tissue culture incubator with 5% CO_2 and 37°C for 1 hour, with periodic mixing every 5-10 minutes.

A 6- well plate was coated with coating media containing 10% Horse Serum (HS) (Wisent, 065250) in DMEM for 30 minutes. The coating media was replaced with 2 mL of unsupplemented DMEM, and the plate was placed in the incubator to preheat the media. After the digestion was complete,

a large bore glass pipette that is coated with coating media was used to transfer the EDL into the 6-well plate. Myofibers were mechanically dissociated by using the large bore glass pipetted and pipetting the EDL up and down. For the 0-hour time point, a subset of myofibers were transferred on a fresh 24-well plate and fixed immediately with 4% PFA. The remaining myofibers were incubated in the unsupplemented DMEM for 1 hour at 5% CO_2 and 37°C. The DMEM was then removed and replaced with 2mL of pre-heated myofiber growth media (15% FBS, 1% chick embryo extract, 1% penicillin/streptomycin and 5 ng/mL of bFGF in DMEM).

Immunofluorescence of EDL Myofibers

EDL myofibers were fixed at the selected times after isolation with 400 µL of 4% PFA in PBS for 5 minutes at RT and then transferred using a small bore glass pipette into a 24 well plate. Myofibers were washed with 400 µL of PBS three times. Myofibers were then permeabilized and blocked at the same time with 400 µL of blocking buffer (2% BSA, 6% HS, 10% GS, 1% Triton X-100, 0.1 M Glycine) for one hour at room temperature. Blocking buffer was then replaced with 200 µL of primary antibody master mix diluted in blocking buffer and incubated over night at 4 °C. After the primary antibody incubation, myofibers were washed three times with 400 µL of 0.1% Triton X-100 in PBS. Next, the samples were incubated with secondary antibody diluted in blocking buffer for 1 hour shielded from light at RT. Then, myofibers were washed three times with 400 µL of 0.1% Triton X-100 in PBS. Finally, myofibers were transferred onto a microscope slide, excess liquid was removed and mounting solution with DAPI was added.

Immunofluorescent Staining of TA Muscle Cross Sections

TA muscle of the mice was dissected and fixed with 0.5% PFA in PBS for 2 hours at 4 °C. PFA was then removed and 20% sucrose in H_2O was added to the muscle and incubated at 4 °C overnight. The TA muscle was then positioned in aluminum foil cups with OCT (Optimal Cutting Temperature) solution, and the muscle was frozen with liquid nitrogen-cooled isopentane. 9 µm thick cross-sections were cut using a cryostat and placed on microscope slides.

For immunofluorescence staining, cross-sections were first permeabilized with 0.5% Triton X for 15 minutes at RT followed by three 5 minute PBS washes. Cross-sections were blocked for 2 hours in blocking solution (3% BSA, 10% GS, 0.1M Glycine, in PBS) in a humid chamber at RT. Primary antibodies were diluted in the blocking solution and were then added and incubated overnight at 4 °C in the humid chamber. The next day, cross-sections were washed with 0.1% Triton X-100 in PBS for 5 minutes on a shaker, three times. After, secondary antibodies diluted 1:400 in the blocking solution were added and incubated for one hour at RT in the dark. Muscle sections were then washed three times with 0.1% Triton X-100 for 5 minutes on a shaker. Lastly, mounting solution with DAPI was added to the sections and cover slips were overlain on the slides to be visualized under the microscope.

Cardiotoxin (CTX) Skeletal Muscle Injury

Skeletal muscle injury was caused by intramuscular injection of cardiotoxin (CTX) (Latoxan, L8102) into the hind limb of mice. 20 minutes prior to muscle injury, mice were subcutaneously injected with 100 µL of carprofen. Mice were anesthetized by isoflurane and intramuscularly injected with 50 µL of 10 µM cardiotoxin. Mice were sacrificed 7 days after the injury for further analysis to measure muscle regeneration.

EchoMRI Readings

Mice were inserted into a size 40 tube and were pushed to the end of the tube using the plastic insert, leaving enough space for the length of the animal's body. The tube containing the mouse was inserted into the EchoMRI and readings were taken with Primary Accumulation set to 1 and the Water Stage set to No. After readings, mice were returned to their home cage.

Metabolic Cage

Metabolic readouts were measured using a Comprehensive Lab Animal Monitoring System (CLAMS) (Columbus Instruments). Mice were placed into individual live-in chambers within a larger environmental control unit. Temperature is maintained between 28 – 30ºC as no bedding or nesting material is provided. A 12-hour light cycle is used for the duration of the experiment. Powdered food is provided *ad libitum* and is measured and recorded throughout the experiment. Animal movement, heat generation and respiration are all recorded throughout the experiment. Readings were taken every 20 minutes.

Heavy Amino Acid Treatment

4-week-old male Balb/c mice were first treated with heavy Arginine (L-Arginine-$^{13}C_6$,$^{15}N_4$ hydrochloride (Millipore Sigma, 608033) for 1 week. The heavy Arginine was dissolved in the drinking water at 1 mg/mL and the mice were provided with 10 mL per mouse of water per day. The water was changed daily. After 7 days, the heavy Arginine water was replaced with normal drinking water for 2 days, then the mice were injected with C26 tumor cells as described above. The tumors were allowed to grow for 7 days with the mice being provided normal drinking water. After the first week of tumor growth, the normal water was replaced with water supplemented with 1 mg/mL of heavy Lysine (L-Lysine, 13C6, 15N2, Hydrochloride (Thermofisher, 88432). Each mouse was provided with 10 mL of water per day and the water was replaced daily. The mice were treated with the heavy Lysine water for 7 days and then euthanized. The whole muscle from the hindlimb and the tumor was isolated.

Extraction and Digestion of Proteins for Total Proteomic Analyses

Proteins from powdered whole tissue were extracted in lysis buffer containing 5% sodium dodecyl sulfate (SDS), 100 mM TRIS pH 7.8. Samples were subsequently heated to 99°C for 10 minutes. The lysate was clarified by centrifugation 14,000 x g for 5 minutes. An aliquot corresponding to 10% of the total volume of lysate was diluted to <1% SDS and used for estimation of protein concentration by bicinchoninic acid assay (BCA). In the remaining sample, protein disulfide bonds were reduced by the addition of tris(2-carboxyethyl)phosphine (TCEP) to a final concentration of 20 mM and incubated at 60°C for 30 minutes. Free cysteines were alkylated using iodoacetamide at a final concentration of 30 mM and subsequent incubation at 37°C for 30 minutes in the dark. An equivalent of 10 µg of total protein was used for proteolytic digestion using suspension trapping (STRAP). In brief, proteins were acidified through the addition of phosphoric acid to a final concentration of 1.3% v/v. The sample was subsequently diluted 6-fold in STRAP loading buffer (9:1 methanol: water in 100 mM TRIS, pH 7.8) and loaded onto an S-TRAP Micro cartridge (Protifi LLC, Huntington NY) and spun at 4000 x g for 2 minutes. Samples were washed three times using 150 µL of STRAP loading buffer. Proteins were then proteolytically digested using trypsin at a 1:10 enzyme to substrate ratio for 2 hours at 47°C. Peptides were sequentially eluted in 50 mM ammonium bicarbonate, 0.1% formic acid in water, and 50% acetonitrile. Peptides were vacuum concentrated and reconstituted in 0.1% formic acid (FA) prior to analysis by LC-MS/MS.

LC-MS/MS Acquisition and Data Analysis

Peptide containing samples were analyzed by data dependent acquisition (DDA-PASEF) using anEvosep One LC system and a Bruker timsTOF HT mass spectrometer. Samples (200ng) were loaded onto Evotips according to the vendor protocol (Evosep). Peptides were separated using the 30 samples per day method and an EV1137 analytical column (Evosep) set to 45°C. Full MS scans were acquired from m/z 100-1,700, between an ion mobility window of 0.6 – 1.6 1/k0 thus filtering for primarily 2+ and 3+ precursor charge states. The 10 most intense ions rPASEF ramp and accumulation times were set to 100 ms and fragmented using a normalized collision energy scaled based on ion mobility – from 20 eV at 0.6 1/k0 to 59 eV at 1.6 1/k0. and the dynamic exclusion was set to 40 s. DDA-PASEF MS raw data was processed with Fragpipe version 22 (https://github.com/Nesvilab/FragPipe)[68] with database searches against a FASTA file containing all reviewed canonical sequences downloaded from UniProt. The enzyme specificity was set to trypsin with a maximum of 2 missed cleavages. Carbamidomethylation of cysteine was set as fixed modification and oxidation of methionine as variable modification. The precursor and product ion mass tolerances were set to 20 ppm. Proteins were quantified by label free quantitation using IonQuant with default settings. In order to estimate the relative amount of a particular protein within the sample we calculated and ranked proteins based on their normalized spectral abundance factor (NSAF) values (https://doi.org/10.1021/pr060161n). Hierarchical clustering was conducted using the normalized protein LFQ abundances as inputs for Instant Clue (http://www.instantclue.uni-koeln.de/) and FragPipe-analyst[69].

Preparation of SMART RNA-Seq library MuSCs and C26 cells

SMART-Seq was performed as previously described with the use of the SMART-Seq HT Kit (TAKARA, 634456)[55]. A 10X SMART-Seq lysis buffer working solution was prepared (95% 10X SMART-Seq lysis buffer, 5% RNase Inhibitor). 1000 MuSCs or C26 tumor cells were sorted by FACS into 10 µL of 1X-SMART Lysis Buffer (1 µL of 10X SMART-Seq lysis buffer working solution + 9 µL ddH_2O). After, 1 µL of 3' SMART-Seq CDS primer II A was added then incubated for 3 minutes at 72 °C in a thermocycler. The template switching master mix (0.7 µL of nuclease free water, 8 µL of one-step buffer, 1 µL SMART-Seq HT oligonucleotide, 0.5 µL RNase inhibitors, 0.3 µL of SeqAMP DNA polymerase and 2 µL of SMARTscribe reverse transcriptase) was prepared and 12.5 µL was added. The cDNA was amplified for 11 cycles as previously described[55]. cDNA was purified with AmpureXP at a 1:1 ratio (v/v). The beads were washed twice with 200 µL of 80% ethanol and the DNA was then eluted with 18 µL of elution buffer. The cDNA was then quantified with a Quant-IT Picogreen dsDNA Assay Kit (Invitrogen, P7589).

Sequencing ready libraries were prepared with Nextera XT Library Prep Kit (Illumina, FC-131-1024) as previously described[55]. In brief, 250 pg of cDNA in a volume of 1.25 µL was transferred to a fresh microtube. 2.5 µL of Tagment DNA (TD) buffer and 1.25 µL Amplicon Tagment Mix (ATM) Buffer were added for a total of 5 µL volume. The cDNA was incubated at 55 °C for 5 minutes in a thermocycler. Immediately after, 1.25 µL of NT Buffer was added and incubated at least 5 minutes at RT. Next, 3.75 µL of NPM PCR master mix, 1.25 µL each of an i7 and an i5 index from the Nextera XT index adaptor kit (Illumina, FC-131–2001) were added for a total of 12.5 µL. The samples were then PCR amplified for 12 cycles as previously described[55]. Lastly, the PCR amplified libraries were purified, and size selected with 0.85X ratio (v/v) AmpureXP beads and were sequenced.

ATAC-Seq of MuSCs

OMNI ATAC-Seq was performed on 5000 freshly sorted MuSCs from 4-month-old healthy control and tumor bearing female mice, as previously described[36]. MuSCs were FACS sorted into 30 µL of ATAC lysis buffer (10 mM Tris-HCl, 10 mM NaCl, 3 mM $MgCl_2$, 0.1% Tween-20, 0.1% NP-40 and 0.01% Digitonin (Promega, G9441)) and incubated on ice for 5 minutes and then at RT for 3 minutes. Cells were then washed with 100 µL of 10 mM Tris-HCl (pH 7.5), 10 Mm NaCl, 3 mM $MgCl_2$ and 0.1% Tween-20, and centrifuged at 800g for 10 minutes. The supernatant was removed and the pellet was resuspended in 10 µL of transposition mixture (5 µL TD buffer, 3.2 µL PBS, 0.89 µL Tn5 (Illumina, 20034197), 0.1% Tween-20, 0.01% Digitonin and 0.75 µL nuclease free water) and incubated at 37 °C for 25 minutes. DNA Purification was performed using a QIAquick PCR Purification Kit (Qiagen, 28,104) according to the manufacturer's guidelines and eluted in 20 µL of elution buffer.

Indices were incorporated by adding 30 µL of the PCR reaction mix (10 µL Q5 buffer, 10 µL Q5 enhancer, 1 µL dNTPs, 2.5 µL i7 index, 2.5 µL i5 index, 3.5 µL nuclease free water, 0.5 µL Q5 High Fidelity DNA polymerase). PCR amplification was performed using the previously described conditions for 12 cycles[36]. The libraries were size selected and purified with Ampure XP beads at a 1:0.85 (v:v) ratio. Samples were sequenced with NovaSeq6000 Sprime, Paired End (PE) 150bp.

Single myofiber RNA-Seq

Single myofiber RNA-Seq (smfRNA-Seq) was performed on EDL myofibers isolated from 4-month-old male and female, healthy control and tumor bearing mice. The procedure was performed as previously described using the SMART-Seq HT Kit and Nextera XT Library Prep Kit[18]. After the dissociation of the myofibers, a coated small-bore glass pipette was used to transfer the myofibers into a 6-well plate containing PBS and a single myofiber was selected and transferred into a 0.2 mL PCR tube. PCR tube was then visualized under the microscope to ensure the selection of one myofiber. The excess PBS was then removed while visualizing under the microscope. 1X SMART lysis buffer was prepared as described in the section, SMART RNA-Seq library preparation of MuSCs. Then 10 µL of the 1X Lysis Buffer was added to the PCR tube containing the myofiber. The fiber was pipetted up and down and lysed on ice for 5 minutes, with vortexing as needed. The sample was then spun down to remove the residual fiber pieces. While visualizing under the microscope, the supernatant was transferred to a new 0.2 mL PCR tube. The cDNA library preparation was performed as described in the above section, SMART RNA-Seq library preparation of MuSCs except for SMART cDNA amplification being 12 cycles. The rest of the library preparation using the Nextera XT library prep kit was performed as described in the previous sections. n=3 RNA-Seq of myofibers was performed to have enough samples for downstream analysis.

EdU Incorporation Assay

EdU incorporation assay was performed using the Click-It Plus EdU Alexa Fluor 555 Imaging Kit (Invitrogen, C10638) according to the manufacturer's guidelines. Cells were seeded into chamber slides prior to EdU Assay. Briefly, 10 µM of EdU was added to the growth media of cultured cells for 12 hours. Following the incubation period, media was removed, and the cells were washed with PBS three times. The cells were then fixed with 3.2% PFA and EdU staining was performed as described by the manufacturer.

RNA-seq Analysis

Single-end RNA-seq reads were quantified with Kallisto v0.46.1 (parameters: –single –fragment-length 200 –sd 20)[70]. Ensembl gene annotations, release 96, were used to create an index for Kallisto[71]. Transcript-level abundance estimates were collapsed to the gene level using "tximport"[70]. Pseudoalignments constructed by kallisto were converted to bigwigs using bamCoverage (version 3.5.1)[72]. Counts were normalized to RPM.

Differentially expressed genes were identify using DESeq2[73]. P values were adjusted for multiple testing using the Independent Hypothesis Weighting procedure[74].

Gene set enrichment analysis was performed using fgsea, the log fold changes, and the Hallmark gene sets collection from Molecular Signatures Database (MsigDB) (https://doi.org/10.1101/060012)[75,76]. Library size normalized gene counts were visualized with ComplexHeatmap[77].

ATAC-Seq Analysis

Adapters were removed from raw ATAC-seq reads using Trimmomatic (version 0.39, parameters: LEADING:10 TRAILING:10 MINLEN:50)[78]. Paired reads were aligned to mm10 using BWA-MEM (version 0.7.17). Samtools was used to index and filter (version 1.16.1, mapping quality > 30)[79]. Duplicated reads were removed using Picard (version 3.1.0). ATAC-seq peaks were called with MACS3 (version 3.0.1, parameters: callpeak, -g mm, -q 0.05)[80].

The summits from each sample are pooled and summits closer to 250 bps are merged. Then, the coordinates are extended 250 bps from the center. Read counts are retrieved from the bam files using featureCounts (version: 2.1.1, -p -F SAF --fracOverlap 0.2)[81].

Differentially bound peaks were identify using DESeq2[73]. P values were adjusted for multiple testing using the Independent Hypothesis Weighting procedure[74]. Peaks were associated to the genes with the closest TSS. Gene set enrichment analysis was performed as described before.

ATAC-seq samples were merged by condition (control and cachexia). Correction of Tn5 insertion bias and calculation of footprint scores were performed using TOBIAS (subcommands: ATACorrect and FootprintScores, with defaults options)[82]. Differentially bound motifs were estimated using TOBIAS (subcommand: BINDetect, defaults options) the Jaspar database (collection: core, vertebrates, non redundant)[83].

Quantification and statistical analysis

Statistical analyses were performed using Prism10 (Graphpad). All data is presented as mean ± SD. When two independent groups were compared an unpaired two-tailed t-tests was used. When multiple groups were compared, analysis was done using a 2-way ANOVA. Exact p values are found within the relevant figure panel and a p-value of < 0.05 was considered to be significant. Sample sizes for each experiment are described in the corresponding figure legend.

Data Availability

All sequencing data generated in this study were deposited to the Gene Expression Omnibus under the super series GSE310038. Individual accession numbers for the RNA-Seq and ATAC-Seq data are GSE309918 and GSE309918 respectively. The token for reviewers to access the data is: ynudyeawhperpgh

Acknowledgements

We thank Dr. Vera Tang and the Flow Core facility at the University of Ottawa for their help with Fluorescence Activated Cell Sorting and Flow Cytometry analysis. We would also like to thank

the Animal Behaviour and Physiology Core, funded by the University of Ottawa Faculty of Medicine, for their assistance with the EchoMRI and metabolic cage data. We thank Mrs. Jothi Krishnamoorthy for excellent technical assistance in some experiments. Cell lines with gene disruptions were generated at the Genomic Engineering and Molecular Biology (GEMb) core facility in the Faculty of Medicine at the University of Ottawa (RRID: SCR_022954). The GEMb facility is supported by CFI-36490, CFI-37607 and CFI-36940. LentiCRISPRv2GFP was a gift from David Feldser (Addgene plasmid # 82416; http://n2t.net/addgene:82416; RRID:Addgene_82416). This work was supported by a Molecular and Regenerative Medicine Pilot Grant Program from the Lady Davis Institute, Jewish General Hospital to V.D.S and A.E.K, as well as from Canadian Institutes of Health Research [CIHR; PJT-178173 and PJT-168864]to A.E.K and Canadian Institutes of Health Research [PJT-190082 and PJT-496845] to V.D.S.

Author Contributions

Conceptualization: D.M.B, A.E.K and V.D.S.; Methodology: D.M.B, K.S, V.R, F.L, A.H.C, D.Q, S.H and H.H.K; Visualization: D.M.B, V.D.S, and A.H.C.; Investigation: D.M.B, A.H.C, and V.D.S; Computational Analysis: A.H.C; Writing manuscript: D.M.B and V.D.S; Supervision: V.D.S, H.N, and C.B.; Funding Acquisition: V.D.S.; Resources: V.D.S, G.B, M.A.R, Y.Y, A.J.A; Reviewing/editing: D.M.B, K.S, F.L and V.D.S.

Competing Interests

The authors declare no competing interests.

References

1 Aversa, Z., Costelli, P. & Muscaritoli, M. Cancer-induced muscle wasting: latest findings in prevention and treatment. *Ther Adv Med Oncol* **9**, 369-382 (2017). https://doi.org/10.1177/1758834017698643

2 Setiawan, T. *et al.* Cancer cachexia: molecular mechanisms and treatment strategies. *J Hematol Oncol* **16**, 54 (2023). https://doi.org/10.1186/s13045-023-01454-0

3 Fearon, K. *et al.* Definition and classification of cancer cachexia: an international consensus. *Lancet Oncol* **12**, 489-495 (2011). https://doi.org/10.1016/S1470-2045(10)70218-7

4 Argiles, J. M., Stemmler, B., Lopez-Soriano, F. J. & Busquets, S. Inter-tissue communication in cancer cachexia. *Nat Rev Endocrinol* **15**, 9-20 (2018). https://doi.org/10.1038/s41574-018-0123-0

5 Caillet, P. *et al.* Association between cachexia, chemotherapy and outcomes in older cancer patients: A systematic review. *Clin Nutr* **36**, 1473-1482 (2017). https://doi.org/10.1016/j.clnu.2016.12.003

6 Ali, R. *et al.* Lean body mass as an independent determinant of dose-limiting toxicity and neuropathy in patients with colon cancer treated with FOLFOX regimens. *Cancer Med* **5**, 607-616 (2016). https://doi.org/10.1002/cam4.621

7 McGovern, J., Dolan, R. D., Skipworth, R. J., Laird, B. J. & McMillan, D. C. Cancer cachexia: a nutritional or a systemic inflammatory syndrome? *Br J Cancer* **127**, 379-382 (2022). https://doi.org/10.1038/s41416-022-01826-2

8 Deng, M. *et al.* Inflammation-associated intramyocellular lipid alterations in human pancreatic cancer cachexia. *J Cachexia Sarcopenia Muscle* **15**, 1283-1297 (2024). https://doi.org/10.1002/jcsm.13474

9 Hamarsheh, S., Gross, O., Brummer, T. & Zeiser, R. Immune modulatory effects of oncogenic KRAS in cancer. *Nat Commun* **11**, 5439 (2020). https://doi.org/10.1038/s41467-020-19288-6

10 Grivennikov, S. I., Greten, F. R. & Karin, M. Immunity, inflammation, and cancer. *Cell* **140**, 883-899 (2010). https://doi.org/10.1016/j.cell.2010.01.025

11 Mariean, C. R., Tiuca, O. M., Mariean, A. & Cotoi, O. S. Cancer Cachexia: New Insights and Future Directions. *Cancers (Basel)* **15** (2023). https://doi.org/10.3390/cancers15235590

12 Lim, S., Brown, J. L., Washington, T. A. & Greene, N. P. Development and progression of cancer cachexia: Perspectives from bench to bedside. *Sports Med Health Sci* **2**, 177-185 (2020). https://doi.org/10.1016/j.smhs.2020.10.003

13 Fearon, K. C., Glass, D. J. & Guttridge, D. C. Cancer cachexia: mediators, signaling, and metabolic pathways. *Cell Metab* **16**, 153-166 (2012). https://doi.org/10.1016/j.cmet.2012.06.011

14 Neyroud, D., Nosacka, R. L., Judge, A. R. & Hepple, R. T. Colon 26 adenocarcinoma (C26)-induced cancer cachexia impairs skeletal muscle mitochondrial function and content. *J Muscle Res Cell Motil* **40**, 59-65 (2019). https://doi.org/10.1007/s10974-019-09510-4

15 Judge, S. M. *et al.* Genome-wide identification of FoxO-dependent gene networks in skeletal muscle during C26 cancer cachexia. *BMC Cancer* **14**, 997 (2014). https://doi.org/10.1186/1471-2407-14-997

16 Bosaeus, I., Daneryd, P., Svanberg, E. & Lundholm, K. Dietary intake and resting energy expenditure in relation to weight loss in unselected cancer patients. *Int J Cancer* **93**, 380-383 (2001). https://doi.org/10.1002/ijc.1332

17 Berriel Diaz, M., Rohm, M. & Herzig, S. Cancer cachexia: multilevel metabolic dysfunction. *Nat Metab* **6**, 2222-2245 (2024). https://doi.org/10.1038/s42255-024-01167-9

18 Blackburn, D. M. *et al.* High-resolution genome-wide expression analysis of single myofibers using SMART-Seq. *J Biol Chem* **294**, 20097-20108 (2019). https://doi.org/10.1074/jbc.RA119.011506

19 Pettersen, I. K. N. *et al.* Upregulated PDK4 expression is a sensitive marker of increased fatty acid oxidation. *Mitochondrion* **49**, 97-110 (2019). https://doi.org/10.1016/j.mito.2019.07.009

20 Fujita, M. *et al.* Upregulation of fatty acyl-CoA thioesterases in the heart and skeletal muscle of rats fed a high-fat diet. *Biol Pharm Bull* **34**, 87-91 (2011). https://doi.org/10.1248/bpb.34.87

21 Sadaki, S. *et al.* Large Maf transcription factor family is a major regulator of fast type IIb myofiber determination. *Cell Rep* **42**, 112289 (2023). https://doi.org/10.1016/j.celrep.2023.112289

22 Dos Santos, M. *et al.* Opposing gene regulatory programs governing myofiber development and maturation revealed at single nucleus resolution. *Nat Commun* **14**, 4333 (2023). https://doi.org/10.1038/s41467-023-40073-8

23 Morales-Scholz, M. G. *et al.* Muscle fiber type-specific autophagy responses following an overnight fast and mixed meal ingestion in human skeletal muscle. *Am J Physiol Endocrinol Metab* **323**, E242-E253 (2022). https://doi.org/10.1152/ajpendo.00015.2022

24 Cheng, J. *et al.* Effect of isolated AMP deaminase deficiency on skeletal muscle function. *Mol Genet Metab Rep* **1**, 51-59 (2014). https://doi.org/10.1016/j.ymgmr.2013.12.004

25 Boulinguiez, A. *et al.* NR1D1 controls skeletal muscle calcium homeostasis through myoregulin repression. *JCI Insight* **7** (2022). https://doi.org/10.1172/jci.insight.153584

26 Yin, A. *et al.* Chronic hypoxia impairs skeletal muscle repair via HIF-2alpha stabilization. *J Cachexia Sarcopenia Muscle* **15**, 631-645 (2024). https://doi.org/10.1002/jcsm.13436

27 von Maltzahn, J., Chang, N. C., Bentzinger, C. F. & Rudnicki, M. A. Wnt signaling in myogenesis. *Trends Cell Biol* **22**, 602-609 (2012). https://doi.org/10.1016/j.tcb.2012.07.008

28 Vargas-Franco, D. *et al.* The Notch signaling pathway in skeletal muscle health and disease. *Muscle Nerve* **66**, 530-544 (2022). https://doi.org/10.1002/mus.27684

29 Brown, J. L. *et al.* Protein imbalance in the development of skeletal muscle wasting in tumour-bearing mice. *J Cachexia Sarcopenia Muscle* **9**, 987-1002 (2018). https://doi.org/10.1002/jcsm.12354

30 Stearns-Reider, K. M. *et al.* Aging of the skeletal muscle extracellular matrix drives a stem cell fibrogenic conversion. *Aging Cell* **16**, 518-528 (2017). https://doi.org/10.1111/acel.12578

31 Mayhew, D. L., Hornberger, T. A., Lincoln, H. C. & Bamman, M. M. Eukaryotic initiation factor 2B epsilon induces cap-dependent translation and skeletal muscle hypertrophy. *J Physiol* **589**, 3023-3037 (2011). https://doi.org/10.1113/jphysiol.2010.202432

32 Li, T. *et al.* Basic biology and roles of CEBPD in cardiovascular disease. *Cell Death Discov* **11**, 102 (2025). https://doi.org/10.1038/s41420-025-02357-4

33 Sampath, S. C. *et al.* Induction of muscle stem cell quiescence by the secreted niche factor Oncostatin M. *Nat Commun* **9**, 1531 (2018). https://doi.org/10.1038/s41467-018-03876-8

34 Domaniku-Waraich, A. *et al.* Oncostatin M signaling drives cancer-associated skeletal muscle wasting. *Cell Rep Med* **5**, 101498 (2024). https://doi.org/10.1016/j.xcrm.2024.101498

35 Charville, G. W. *et al.* Ex Vivo Expansion and In Vivo Self-Renewal of Human Muscle Stem Cells. *Stem Cell Reports* **5**, 621-632 (2015). https://doi.org/10.1016/j.stemcr.2015.08.004

36 Blackburn, D. M. *et al.* The E3 ubiquitin ligase Nedd4L preserves skeletal muscle stem cell quiescence by inhibiting their activation. *iScience* **27**, 110241 (2024). https://doi.org/10.1016/j.isci.2024.110241

37 Vairapandi, M., Balliet, A. G., Hoffman, B. & Liebermann, D. A. GADD45b and GADD45g are cdc2/cyclinB1 kinase inhibitors with a role in S and G2/M cell cycle checkpoints induced by genotoxic stress. *J Cell Physiol* **192**, 327-338 (2002). https://doi.org/10.1002/jcp.10140

38 Sala, D. *et al.* The Stat3-Fam3a axis promotes muscle stem cell myogenic lineage progression by inducing mitochondrial respiration. *Nat Commun* **10**, 1796 (2019). https://doi.org/10.1038/s41467-019-09746-1

39 Tierney, M. T. *et al.* STAT3 signaling controls satellite cell expansion and skeletal muscle repair. *Nat Med* **20**, 1182-1186 (2014). https://doi.org/10.1038/nm.3656

40 Zhu, H. *et al.* STAT3 Regulates Self-Renewal of Adult Muscle Satellite Cells during Injury-Induced Muscle Regeneration. *Cell Rep* **16**, 2102-2115 (2016). https://doi.org/10.1016/j.celrep.2016.07.041

41 Catarinella, G. *et al.* STAT3 inhibition recovers regeneration of aged muscles by restoring autophagy in muscle stem cells. *Life Sci Alliance* **7** (2024). https://doi.org/10.26508/lsa.202302503

42 McKay, S. *et al.* Pro-inflammatory cytokines induce c-fos expression followed by IL-6 release in human airway smooth muscle cells. *Mediators Inflamm* **10**, 135-142 (2001). https://doi.org/10.1080/09629350124155

43 von Maltzahn, J., Jones, A. E., Parks, R. J. & Rudnicki, M. A. Pax7 is critical for the normal function of satellite cells in adult skeletal muscle. *Proc Natl Acad Sci U S A* **110**, 16474-16479 (2013). https://doi.org/10.1073/pnas.1307680110

44 Ganassi, M. *et al.* Myogenin promotes myocyte fusion to balance fibre number and size. *Nat Commun* **9**, 4232 (2018). https://doi.org/10.1038/s41467-018-06583-6

45 Soleimani, V. D. *et al.* Snail regulates MyoD binding-site occupancy to direct enhancer switching and differentiation-specific transcription in myogenesis. *Mol Cell* **47**, 457-468 (2012). https://doi.org/10.1016/j.molcel.2012.05.046

46 Groarke, J. D. *et al.* Ponsegromab for the Treatment of Cancer Cachexia. *N Engl J Med* **391**, 2291-2303 (2024). https://doi.org/10.1056/NEJMoa2409515

47 Liu, L., Ye, Y. & Zhu, X. MMP-9 secreted by tumor associated macrophages promoted gastric cancer metastasis through a PI3K/AKT/Snail pathway. *Biomed Pharmacother* **117**, 109096 (2019). https://doi.org/10.1016/j.biopha.2019.109096

48 Scannevin, R. H. *et al.* Discovery of a highly selective chemical inhibitor of matrix metalloproteinase-9 (MMP-9) that allosterically inhibits zymogen activation. *J Biol Chem* **292**, 17963-17974 (2017). https://doi.org/10.1074/jbc.M117.806075

49 Kunz, H. E. *et al.* Skeletal muscle mitochondrial dysfunction and muscle and whole body functional deficits in cancer patients with weight loss. *J Appl Physiol (1985)* **132**, 388-401 (2022). https://doi.org/10.1152/japplphysiol.00746.2021

50 Abrigo, J. *et al.* Role of Oxidative Stress as Key Regulator of Muscle Wasting during Cachexia. *Oxid Med Cell Longev* **2018**, 2063179 (2018). https://doi.org/10.1155/2018/2063179

51 Delfinis, L. J. *et al.* Muscle weakness precedes atrophy during cancer cachexia and is linked to muscle-specific mitochondrial stress. *JCI Insight* **7** (2022). https://doi.org/10.1172/jci.insight.155147

52 Tisdale, M. J. Cancer cachexia: metabolic alterations and clinical manifestations. *Nutrition* **13**, 1-7 (1997). https://doi.org/10.1016/s0899-9007(96)00313-9

53 Riparini, G. *et al.* Epigenetic dysregulation in aged muscle stem cells drives mesenchymal progenitor expansion via IL-6 and Spp1 signaling. *Nat Aging* (2025). https://doi.org/10.1038/s43587-025-01002-0

54 Massenet, J. *et al.* Epigenetic control of myogenic identity of human muscle stem cells in Duchenne muscular dystrophy. *iScience* **27**, 111350 (2024). https://doi.org/10.1016/j.isci.2024.111350

55 Lazure, F. *et al.* Transcriptional reprogramming of skeletal muscle stem cells by the niche environment. *Nat Commun* **14**, 535 (2023). https://doi.org/10.1038/s41467-023-36265-x

56 Wang, D. *et al.* GDF15 promotes weight loss by enhancing energy expenditure in muscle. *Nature* **619**, 143-150 (2023). https://doi.org/10.1038/s41586-023-06249-4

57 Tian, T. *et al.* Emerging Roles of GDF15 in Metabolic and Cardiovascular Diseases. *Research (Wash D C)* **8**, 0832 (2025). https://doi.org/10.34133/research.0832

58 Li, L. *et al.* GDF15 knockdown suppresses cervical cancer cell migration in vitro through the TGF-beta/Smad2/3/Snail1 pathway. *FEBS Open Bio* **10**, 2750-2760 (2020). https://doi.org/10.1002/2211-5463.13013

59 Asadullah *et al.* MMP9 shapes cell mechanics to enable collective invasion in cancer. *NPJ Syst Biol Appl* **11**, 120 (2025). https://doi.org/10.1038/s41540-025-00601-2
60 Khalili-Tanha, G., Radisky, E. S., Radisky, D. C. & Shoari, A. Matrix metalloproteinase-driven epithelial-mesenchymal transition: implications in health and disease. *J Transl Med* **23**, 436 (2025). https://doi.org/10.1186/s12967-025-06447-w
61 Moore-Smith, L. D., Isayeva, T., Lee, J. H., Frost, A. & Ponnazhagan, S. Silencing of TGF-beta1 in tumor cells impacts MMP-9 in tumor microenvironment. *Sci Rep* **7**, 8678 (2017). https://doi.org/10.1038/s41598-017-09062-y
62 Lazure, F. *et al.* Myf6/MRF4 is a myogenic niche regulator required for the maintenance of the muscle stem cell pool. *EMBO Rep* **21**, e49499 (2020). https://doi.org/10.15252/embr.201949499
63 Concordet, J. P. & Haeussler, M. CRISPOR: intuitive guide selection for CRISPR/Cas9 genome editing experiments and screens. *Nucleic Acids Res* **46**, W242-W245 (2018). https://doi.org/10.1093/nar/gky354
64 Walter, D. M. *et al.* Systematic In Vivo Inactivation of Chromatin-Regulating Enzymes Identifies Setd2 as a Potent Tumor Suppressor in Lung Adenocarcinoma. *Cancer Res* **77**, 1719-1729 (2017). https://doi.org/10.1158/0008-5472.CAN-16-2159
65 Sanjana, N. E., Shalem, O. & Zhang, F. Improved vectors and genome-wide libraries for CRISPR screening. *Nat Methods* **11**, 783-784 (2014). https://doi.org/10.1038/nmeth.3047
66 Clement, K. *et al.* CRISPResso2 provides accurate and rapid genome editing sequence analysis. *Nat Biotechnol* **37**, 224-226 (2019). https://doi.org/10.1038/s41587-019-0032-3
67 Brinkman, E. K., Chen, T., Amendola, M. & van Steensel, B. Easy quantitative assessment of genome editing by sequence trace decomposition. *Nucleic Acids Res* **42**, e168 (2014). https://doi.org/10.1093/nar/gku936
68 Yu, F. *et al.* Fast Quantitative Analysis of timsTOF PASEF Data with MSFragger and IonQuant. *Mol Cell Proteomics* **19**, 1575-1585 (2020). https://doi.org/10.1074/mcp.TIR120.002048
69 Hsiao, Y. *et al.* Analysis and Visualization of Quantitative Proteomics Data Using FragPipe-Analyst. *J Proteome Res* **23**, 4303-4315 (2024). https://doi.org/10.1021/acs.jproteome.4c00294
70 Bray, N. L., Pimentel, H., Melsted, P. & Pachter, L. Near-optimal probabilistic RNA-seq quantification. *Nat Biotechnol* **34**, 525-527 (2016). https://doi.org/10.1038/nbt.3519
71 Dyer, S. C. *et al.* Ensembl 2025. *Nucleic Acids Res* **53**, D948-D957 (2025). https://doi.org/10.1093/nar/gkae1071
72 Ramirez, F. *et al.* deepTools2: a next generation web server for deep-sequencing data analysis. *Nucleic Acids Res* **44**, W160-165 (2016). https://doi.org/10.1093/nar/gkw257

73 Love, M. I., Huber, W. & Anders, S. Moderated estimation of fold change and dispersion for RNA-seq data with DESeq2. *Genome Biol* **15**, 550 (2014). https://doi.org/10.1186/s13059-014-0550-8

74 Ignatiadis, N., Klaus, B., Zaugg, J. B. & Huber, W. Data-driven hypothesis weighting increases detection power in genome-scale multiple testing. *Nat Methods* **13**, 577-580 (2016). https://doi.org/10.1038/nmeth.3885

75 Subramanian, A. *et al.* Gene set enrichment analysis: a knowledge-based approach for interpreting genome-wide expression profiles. *Proc Natl Acad Sci U S A* **102**, 15545-15550 (2005). https://doi.org/10.1073/pnas.0506580102

76 Mootha, V. K. *et al.* PGC-1alpha-responsive genes involved in oxidative phosphorylation are coordinately downregulated in human diabetes. *Nat Genet* **34**, 267-273 (2003). https://doi.org/10.1038/ng1180

77 Gu, Z., Eils, R. & Schlesner, M. Complex heatmaps reveal patterns and correlations in multidimensional genomic data. *Bioinformatics* **32**, 2847-2849 (2016). https://doi.org/10.1093/bioinformatics/btw313

78 Bolger, A. M., Lohse, M. & Usadel, B. Trimmomatic: a flexible trimmer for Illumina sequence data. *Bioinformatics* **30**, 2114-2120 (2014). https://doi.org/10.1093/bioinformatics/btu170

79 Danecek, P. *et al.* Twelve years of SAMtools and BCFtools. *Gigascience* **10** (2021). https://doi.org/10.1093/gigascience/giab008

80 Zhang, Y. *et al.* Model-based analysis of ChIP-Seq (MACS). *Genome Biol* **9**, R137 (2008). https://doi.org/10.1186/gb-2008-9-9-r137

81 Liao, Y., Smyth, G. K. & Shi, W. featureCounts: an efficient general purpose program for assigning sequence reads to genomic features. *Bioinformatics* **30**, 923-930 (2014). https://doi.org/10.1093/bioinformatics/btt656

82 Bentsen, M. *et al.* ATAC-seq footprinting unravels kinetics of transcription factor binding during zygotic genome activation. *Nat Commun* **11**, 4267 (2020). https://doi.org/10.1038/s41467-020-18035-1

83 Rauluseviciute, I. *et al.* JASPAR 2024: 20th anniversary of the open-access database of transcription factor binding profiles. *Nucleic Acids Res* **52**, D174-D182 (2024). https://doi.org/10.1093/nar/gkad1059

Figure 1: C26 tumors induce cachexia in male and female mice

(A) Schematic of the overall experimental design for C26 tumor growth and muscle analysis. **(B)** Image of female healthy control and tumor bearing Balb/c mice. **(C)** Line chart of the change in body mass in female mice as tumor develops. n = 5 mice. **(D)** Binning of the CSA of myofibers from healthy control and tumor bearing female mice. Data is presented as a percentage of all myofibers that measure within the marked range in area. n = 5 mice. **(E)** Representative image of a TA cross section, scale bar = 70μm. **(F)** Percentage of fat mass in male healthy control and cachectic mice, measured at endpoint (16-19 days post C26 injection). n = 6 controls, and 20 tumor bearing mice. **(G)** Percentage of lean mass in male healthy control and cachectic mice, measured at endpoint (16-19 days post C26 injection). n = 6 controls, and 20 tumor bearing mice. **(H)** The body weight of male mice after removal of tumors. n = 6 controls, and 20 tumor bearing mice. Daily measured food consumption in male mice in the **(I)** first week, **(J)** second week, and **(K)** third week post tumor cell injection. n = 6 mice. Average daily RER value quantified in male mice in the **(L)** first week, **(M)** second week, and **(N)** third week post C26 injection. n = 6 mice.

Figure 2: Cancer alters the myofiber transcriptome

(A) Schematic of the experimental design, where the RNA from individual myofibers isolated from tumor bearing mice and healthy controls is used to generate single myofiber RNA-Seq libraries, n=4 mice per condition and sex; 1 myofiber per mouse. **(B)** Volcano plot of sequenced female myofibers from control and tumor bearing mice, genes are labelled as significantly different if the adj. pvalue ≤ 0.05. **(C)** Volcano plot of sequenced male myofibers from control and tumor bearing mice, genes are labelled as significantly different if the adj. pvalue ≤ 0.05. **(D)** Heatmaps of the differentially expressed genes (adj. pvalue ≤ 0.05) of control vs cachexia myofiber samples from both female and male mice. **(E)** Heatmaps of the top 100 differentially expressed genes (adj. pvalue ≤ 0.05) of control vs cachexia myofiber samples from both female and male mice. **(F)** PCA plot of myofibers from control and tumor bearing female mice. **(G)** PCA plot of myofibers from control and tumor bearing male mice. **(H)** Pearson correlations between the sequenced female myofiber samples. **(I)** Pearson correlations between the sequenced male myofiber samples. **(J)** Bar graphs of the expression of PDK4 and **(K)** Acot 2 in female myofibers. **(L)** Bar graphs of the expression of PDK4 and **(M)** Acot 2 in male myofibers. **(N)** Mafa expression in female myofibers. **(O)** Bar graph of the RPM value of Map1lc3b in female myofibers. **(P)** RPM expression of Ampd1 in male myofibers. **(Q)** Mrln expression in male myofibers. **(R)** Bar graph of the top ten most upregulated Hallmark pathways, in terms of enrichment score, from control vs tumor female myofibers. **(S)** Bar graph of the top ten most downregulated Hallmark pathways, in terms of enrichment score, from control vs tumor female myofibers. **(T)** Bar graph of the top ten most upregulated Hallmark pathways, in terms of enrichment score, from control vs tumor male myofibers. **(U)** Bar graph of the top ten most significantly upregulated pathways from microarray data of skeletal muscle biopsies from cachectic vs non cachectic pancreatic ductal adenocarcinoma patients. Data was retrieved from GSE130563[14].

Figure 3: MuSCs are transcriptionally deregulated in cachexia

(A) Schematic of the experimental design where pure populations of muscle stem cells are isolated from healthy controls and tumor bearing mice. The RNA from these cells is used to generate sequencing libraries. **(B)** Volcano plot of the female MuSCs control vs tumor transcripts. **(C)** Volcano plot of the male MuSCs control vs tumor transcripts. **(D)** Heatmaps of the differentially expressed genes (adj. pvalue ≤ 0.05) of control vs tumor MuSC samples from both female and male mice. **(E)** Heatmaps of the top 100 differentially expressed genes (adj. pvalue ≤ 0.05) of control vs tumor MuSC samples from both female and male mice. **(F)** PCA plot of female MuSCs from control and tumor bearing mice. **(G)** PCA plot of male MuSCs from control and tumor bearing mice. **(H)** Pearson correlations between the sequenced female MuSC samples. **(I)** Pearson correlations between the sequence male MuSC samples. **(J)** RPM expression of Col3a1 in female MuSCs. **(K)** RPM expression of Eif2s2 in female MuSCs. **(L)** RPM expression of Cebpd in female MuSCs. **(M)** RPM expression of MT1 in female MuSCs. **(N)** RPM expression of OSMR in male MuSCs. **(O)** RPM expression of Chrdl2 in male MuSCs. **(P)** RPM expression of Gadd45g in male MuSCs. **(Q)** RPM expression of STAT3 in male MuSCs. **(R)** Bar graph of the top ten most upregulated Hallmark pathways, in terms of enrichment score, from control vs tumor female MuSCs. **(S)** Bar graph of the top ten most downregulated Hallmark pathways, in terms of enrichment score, from control vs tumor female MuSCs. **(T)** Bar graph of the top ten most upregulated Hallmark pathways, in terms of enrichment score, from control vs tumor male MuSCs. **(U)** Bar graph of the top ten most downregulated Hallmark pathways, in terms of enrichment score, from control vs tumor female MuSCs.

Figure 4: Epigenetic landscape is greatly altered in MuSCs from tumor bearing mice

(A) Schematic of the experimental design where MuSCs from healthy and tumor bearing mice are FACS isolated. The DNA is tagmented and ATAC-Seq libraries are created from the isolated MuSCs. **(B)** Volcano plot of the mapped peaks between MuSCs from healthy controls and cachectic mice. **(C)** PCA plot of the control and cachectic MuSCs. **(D)** The top ten most enriched pathways from the differentially accessible peaks between control and cachectic MuSCs. IGV tracks of ATAC-seq peaks at the **(E)** Myogenin, **(F)** CCND1, and **(G)** RPS2 genes. **(H)** Volcano plot of the changes in transcription factor binding in the differential peaks between control and cachectic MuSCs. Bar graphs of the number of transcription factor binding sites in control and cachectic MuSC peaks for **(I)** FOSL:JUND, **(J)** ATF4, **(K)** MyoD, **(L)** Myogenin, **(M)** Myf5, and **(N)** Myf6.

Figure 5: MuSCs from tumor bearing mice show a functional decline

(A) Immunofluorescence staining of freshly isolated myofibers from control and tumor bearing female mice for PAX7. Scale bar = 30µm, n = 4 mice. **(B)** Bar graph of the average number of MuSCs on freshly isolated myofibers from control and tumor bearing female mice. **(C)** Immunofluorescence staining for PAX7 and Laminin on TA cross sections from control and tumor bearing female mice. Scale bar = 30 µm, n = 6 control mice and 5 tumor bearing mice. **(D)** Bar graph of the average number of MuSCs/mm2 in TA cross sections from control and tumor bearing female mice. **(E)** Representative images of TA cross sections 7 days post injury (7DPI) from healthy control and tumor bearing female mice. Sections were stained for PAX7 and Laminin. Scale bar = 30 µm. n = 3 mice**. (F)** CSA measurements of 7DPI TA myofibers in control and tumor bearing female mice. **(G)** Quantification of the number of MuSCs/mm2 in TA cross sections**. (H)** Immunofluorescence staining of 48-hour cultured myofibers, from control and tumor bearing female mice, for PAX7 and MyoD. Scale bar = 30 µm, n = 5 mice. **i.** Bar graph of the average number of MuSCs on 48-hour cultured myofibers from control and tumor bearing female mice. **(J)** Immunofluorescence staining of 72-hour cultured myofibers, from control and tumor bearing female mice, for Myogenin and MyoD. Scale bar = 30 µm, n = 5 control mice, n = 6 tumor bearing mice. **(K)** Bar graph of the average number of MuSCs on 72-hour cultured myofibers from control and tumor bearing female mice. **(L)** Bar graph of the average number of MuSCs on myofibers that were cocultured for 48 hours with either HEK cells or C26 cancer cells, n = 3 mice. **(M)** Bar graph of the average number of MuSCs on myofibers that were cocultured for 72 hours with either HEK cells or C26 cancer cells. **(N)** Representative immunofluorescence images of myofibers cocultured with HEK or C26 cancer cells for 72 hours. Myofibers were stained for PAX7 and MyoD. Scale bar = 20 µm.

Figure 6: C26 cancers cells alter their transcriptome in an *in vivo* environment

(A) Schematic of the experimental design, where C26 cells are transformed to stably express GFP. The cells are injected into both male and female Balb/c mice. The GFP cells are reisolated from the solid tumors and, simultaneously with the *in vitro* cultured cells, RNA-Sequencing libraries are generated. Figure created with Biorender.com. **(B)** FACS plot of No-GFP control, indicating GFP and DAPI intensity. **(C)** FACS plot of GFP C26 solid tumors and gating for the isolation of GFP positive C26 cells. **(D)** PCA plot of RNA-Seq C26 samples from *in vitro* culture, *in vivo* in female mice and *in vivo* in male mice. **(E)** Pearson correlation graph between the *in vitro* and *in vivo* samples. **(F)** Volcano plot of the difference in transcript expression between *in vitro* cultured C26 cells and female *in vivo* C26 cells. **(G)** Volcano plot of the difference in transcript expression between female *in vivo* and male *in vivo* C26 cells. **(H)** Heatmap of differentially expressed genes (adj. pvalue $\leq$ 0.1) between *in vitro* and female *in vivo* C26 cells. **(I)** Heatmap of differentially expressed genes (adj. pvalue $\leq$ 0.1) between female *in vivo* and male *in vivo* C26 cells. **(J)** Bar graph of the top ten most enriched Hallmark pathways between *in vitro* C26 and *in vivo* C26 in female mice. Blue bars represent downregulated pathways; orange bars represent upregulated pathways. **(K)** Bar graph of the top ten most enriched Hallmark pathways between *in vivo* C26 in female mice and *in vivo* C26 in male mice. Blue bars represent downregulated pathways; orange bars represent upregulated pathways.

Figure 7: GDF15 induces SNAI1 in muscle stem cells and blocks differentiation

(A) Membranes from Proteome Profiler Mouse XL Cytokine Array incubated with serum collected from 4-month-old male healthy control balb/c mice and tumor bearing mice 14 days post C26 injection, n = 2 mice. **(B)** Membranes from Proteome Profiler Mouse XL Cytokine Array incubated with serum collected from 4-month-old female healthy control balb/c mice and tumor bearing mice 14 days post C26 injection, n = 2 mice. **(C)** Quantification of MMP9 levels in the serum of male healthy control and tumor bearing mice. Values are normalized and presented as a percentage of the control. n = 2 mice, 4 technical replicates. **(D).** Quantification of MMP9 levels in the serum of female healthy control and tumor bearing mice. Values are normalized and presented as a percentage of the control. n = 2 mice, 4 technical replicates. **(E)** Quantification of GDF15 level in the serum from male healthy control and tumor bearing mice. Values are normalized and presented as a percentage of the control. n = 2 mice, 4 technical replicates. **(F)** Quantification of GDF15 level in the serum from female healthy control and tumor bearing mice. Values are normalized and presented as a percentage of the control. n = 2 mice, 4 technical replicates. Bar graph of the absolute expression of **(G)** Snai1, **(H)** Myogenin, and **(I)** Mymk transcripts (RPM) in MuSCs freshly isolated from female 3-month-old healthy control and tumor bearing mice. **(J)** Representative pictures of isolated EDL myofibers cultured for 24 hours in unsupplemented growth media (15% FBS, 1% P/S, - CEE, - bFGF), normal growth media (15% FBS, 1% P/S, 1% CEE, 5 ng/µL bFGF) and GDF15 supplemented growth media (15% FBS, 1% P/S, 500 ng/µL GDF15, - CEE, - bFGF), GDF15 was added every 12 hours. Myofibers were stained for PAX7 and SNAI1. n = 4 mice. Scale bar = 20 µm. **(K)** Quantification of the average number of MuSCs per EDL myofiber from myofibers cultured for 24 hours in unsupplemented, normal growth and GDF15 treated conditions. **(L)** Quantification of the percentage of high SNAI1 expressing MuSCs per EDL myofiber from myofibers cultured for 24 hours in unsupplemented, normal growth and GDF15 treated conditions. **(M)** Quantification of the average number of MuSCs per EDL myofiber from myofibers cultured for 72 hours in unsupplemented, normal growth and GDF15 treated conditions. **(N)** Representative pictures of isolated EDL myofibers cultured for 72 hours in unsupplemented growth media (15% FBS, 1% P/S, - CEE, - bFGF), normal growth media (15% FBS, 1% P/S, 1% CEE, 5 ng/µL bFGF) and GDF15 supplemented growth media (15% FBS, 1% P/S, 500 ng/µL GDF15, - CEE, - bFGF), GDF15 was added every 12 hours. n = 4 mice. Scale bar = 20 µm. **(O).** Quantification of the fusion index of 3DM myotubes that were treated with siSNAI1 or SiControl. n = 4 biological replicates. **(P).** Representative image of 3DM siSNAI1 and siControl myotubes cultured in normal differentiation media stained for MyHC. **(Q).** Quantification of the fusion index of 3DM myotubes that were treated with siSNAI1 or SiControl and cultured in C26 conditioned differentiation media (CM). n = 4 biological replicates. **(R).** Representative image of 3DM siSNAI1 and SiControl myotubes cultured in C26 conditioned differentiation media (CM) stained for MyHC. **(S).** Representative images of 3DM myotubes cultured with either normal differentiation media or C26 conditioned differentiation media (CM), myotubes were either untreated, treated with siControl or siSNAI1. Cells were stained for Myogenin and Cleaved Caspase 3. n= 4 biological replicates. **(T).** Quantification of the percentage of myogenin expressing nuclei in 3DM myotubes that were untreated, treated with siControl or siSNAI1. Myotubes were cultured for 3 days in either normal differentiation media or C26 conditioned media (CM). **(U).** Quantification of the percentage of Cleaved Caspase 3 expressing nuclei in 3DM myotubes that were untreated, treated with siControl or siSNAI1. Myotubes were cultured for 3 days in either normal differentiation media or C26 conditioned media (CM).

Figure 8: Pharmacological inhibition partially blocks cachexia and rescues the MuSC pool

(A) Quantification of the average number of muscle stem cells per myofiber from Healthy Controls, Crispr Control and GDF15 KO tumor bearing mice. n = 3 Healthy Controls, 6 Crispr Controls and 6 GDF15 KO tumor bearing mice. **(B)** Representative immunofluorescence pictures of freshly isolated EDL myofibers from Healthy Controls, Crispr Control and GDF15 KO tumor bearing mice. Myofibers were stained for PAX7. n = 3 Healthy Controls, 6 Crispr Controls and 6 GDF15 KO tumor bearing mice. Scale bar = 20 μm. **(C)** Quantification of the number of muscle stem cells per mm^2 in TA cross sections from Healthy Controls, Crispr Controls and GDF15 KO tumor bearing mice. **(D)** Representative pictures of immunofluorescence staining of TA cross sections from Healthy Controls, Crispr Controls and GDF15 KO tumor bearing mice. Cross sections were stained for Laminin and PAX7. n = 3 Healthy Controls, 6 Crispr Controls and 6 GDF15 KO tumor bearing mice. Scale bar = 30 μm. **(E).** Quantification of the body mass minus the tumor mass of DMSO or JNJ0966 treated C26 tumor bearing male mice, n = 10 mice per condition. **(F).** Quantification of the tumor mass of DMSO or JNJ0966 treated C26 tumor bearing male mice, n = 10 mice per condition. **(G).** Quantification of the weight of the contralateral uninjured tibialis anterior muscle of DMSO or JNJ0966 treated C26 tumor bearing male mice, n = 10 mice per condition. **(H).** Quantification of the tumor mass of DMSO or JNJ0966 treated C26 tumor bearing male mice, n = 10 mice per condition. **(G).** Quantification of the weight of the tibialis anterior muscle, 7 days post injury, of DMSO or JNJ0966 treated C26 tumor bearing mice, n = 10 mice per condition. **(I).** Binning of the CSA of uninjured TA myofibers from DMSO or JNJ0966 treated tumor bearing male mice. Data is presented as a percentage of all myofibers that measure within the marked range in area. n = 10 mice per condition. **(J).** Representative image of the TA 7DPI from DMSO and JNJ0966 treated C26 tumor bearing mice. Sections are stained with laminin. scale = 50μm. **(K).** Binning of the CSA of injured TA myofibers from DMSO or JNJ0966 treated tumor bearing male mice. Data is presented as a percentage of all myofibers that measure within the marked range in area. n = 10 mice per condition. **(L).** Quantification of the average number of MuSCs per freshly isolated EDL myofiber from DMSO or JNJ0966 treated C26 tumor bearing male mice. n = 8 mice per condition. **(M).** Representative image of freshly isolated EDL myofibers from DMSO and JNJ0966 treated C26 tumor bearing male mice. Myofibers were stained for PAX7. Scale bar = 30μm. **(N).** Quantification of the average number of MuSCs per mm2 in uninjured and 7DPI TA muscle cross sections collected from DMSO or JNJ0966 treated C26 tumor bearing male mice. n = 8 mice per condition. **(O).** Representative image of uninjured and 7DPI TA cross sections from DMSO and JNJ0966 treated C26 tumor bearing male mice. Sections were stained for Laminin and PAX7. Scale bar = 50 μm.

Figure 9: Tumor derived cytokines directly communicate with muscle stem cells inhibiting their myogenic potential and promoting cell death

Summary figure describing how C26 cancer cells adapt to the host *in vivo* environment and produce secreted factors which are known to promote their own growth and survival. These factors enter the circulatory system where they make contact with MuSCs. The signaling induces the EMT program and causes the MuSCs to upregulate SNAI1 and decrease its differentiation potential, reducing the capacity of these cells to fuse and contribute to muscle growth. The MuSCs instead undergo cell death from apoptosis and there is a reduction in the stem cell pool.

Supplemental Information

Multiomic Analysis of Cachectic Mice Reveals Cancer Driven Suppression of Muscle Differentiation

Darren M. Blackburn[1,*], Aldo Hernández-Corchado[2], Korin Sahinyan[2,3], Hedieh Habibi Khorasani[1], Felicia Lazure[4], Vincent Richard[5], Dianbo Qu[9], Shuo Wang[3] Christoph H. Borchers[5-8], Arezu Jahani-Asl[9], Hamed S. Najafabadi[2], Antonis Koromilas[3,6], Vahab D. Soleimani[1,2,*]

[1] Department of Biochemistry, Microbiology & Immunology, University of Ottawa, 451 Smyth Rd, Ottawa, ON, K1H 8M5 Canada

[2] Department of Human Genetics, McGill University, 3640 rue University, Montréal, QC, H3A 0C7, Canada.

[3] Lady Davis Institute for Medical Research, Jewish General Hospital, 3755 Chemin de la Côte-Sainte-Catherine, Montréal QC, H3T 1E2, Canada.

[4] Moffit Cancer Cetner, Tumor Microenvironment and Metastasis Department, Tampa, FL 33612, USA.

[5] Segal Cancer Proteomics Centre, Lady Davis Institute, Jewish General Hospital, McGill University, Montréal, Quebec H3T 1E2, Canada.

[6] Gerald Bronfman Department of Oncology, Lady Davis Institute for Medical Research, Jewish General Hospital, Montréal, QC H3T 1E2, Canada

[7] Division of Experimental Medicine, McGill University, Montréal, QC H4A 3J1, Canada

[8] Department of Pathology, McGill University, Montréal, QC H3A 2B4, Canada

[9] Department of Cellular and Molecular Medicine and University of Ottawa Brain and Mind Research Institute, University of Ottawa, Ottawa, ON, Canada

[*] Corresponding authors: Vahab D Soleimani: Tel: +1 514 340 8222 ext. 26136, vahab.soleimani@uottawa.ca

Darren M Blackburn: Tel: +1 613 809 1759, dblackb3@uottawa.ca

Expanded View Figures 1-8

Expanded View Figure 1: Transcriptional variation between male and female myofibers

a. Bar graph of the gene expression of selected fast and slow myofiber specific genes from all myofibers sequenced in this project (n=8 mice; 1 myofiber/mouse). **b.** Heatmap of the differentially expressed genes (adj. p-value $\leq$ 0.05) between male and female myofibers from tumor bearing (left) and healthy control (right) mice. **c.** Heatmap of the top 100 most differentially expressed genes (adj. p-value $\leq$ 0.05) between male and female myofibers from tumor bearing (left) and healthy control (right) mice. **d.** PCA plot of sequenced single myofibers from healthy 3-month-old male and female mice. **e.** PCA plot of sequenced single myofibers from tumor bearing 3-month-old male and female mice. **f.** Pearson correlation between male and female myofibers isolated from healthy controls. **g.** Pearson correlation between male and female myofibers isolated from tumor bearing mice. **h.** Volcano plot of male vs female myofibers isolated from healthy controls. **i.** Volcano plot of male vs female myofibers isolated from tumor bearing mice. **j.** Scatterplot of the effect of cachexia on transcript levels between male and female myofibers. Comparison between the LFC of all genes of healthy controls vs cachexia in male with the LFC of female healthy controls vs cachexia. **k.** Scatterplot comparing the LFC of healthy controls vs cachexia in male with the LFC of female healthy controls vs cachexia. Only genes that are significantly different (adjusted p-value $\leq$ 0.05) in both groups were plotted.

Expanded View Figure 2: Muscle proteome is significantly altered during cachexia

a. PCA plot of control and cachectic whole muscle. **b.** Pearson correlation between control and cachectic whole muscle samples. **c.** Heatmap of all the significantly different (LFC $\geq$ 1.5 and adjusted p-value $\leq$ 0.05) proteins between control and cachectic muscle. **d.** Volcano plot of the LFC in protein expression between control and cachectic muscle. Significantly different proteins are labelled. **e.** Bar plot of the percentage of peptides containing heavy lysine, heavy arginine, both, or none in the control and cachectic whole muscle and tumor whole tissue samples.

Expanded View Figure 3: Male and female MuSCs have a distinct transcriptomic profile but are similarly affected by cachexia.

a. Heatmap of the differentially expressed genes (adj. p-value ≤ 0.05) between male and female MuSCs from tumor bearing (left) and healthy control (right) mice. **b.** Heatmap of the top 100 most differentially expressed genes (adj. p-value ≤ 0.05) between male and female MuSCs from tumor bearing (left) and healthy control (right) mice. **c.** PCA plot of sequenced MuSCs from healthy 3-month-old male and female mice. **d.** PCA plot of sequenced MuSCs from tumor bearing 3-month-old male and female mice. **e.** Pearson correlation between male and female MuSCs isolated from healthy controls. **f.** Pearson correlation between male and female MuSCs isolated from tumor bearing mice. **g.** Volcano plot of male vs female MuSCs isolated from healthy controls. **h.** Volcano plot of male vs female MuSCs isolated from tumor bearing mice. **i.** Scatterplot of the effect of cachexia on transcript levels between male and female MuSCs. Comparison between the LFC of all genes of healthy controls vs cachexia in male with the LFC of female healthy controls vs cachexia. **j.** Scatterplot comparing the LFC of healthy controls vs cachexia in male with the LFC of female healthy controls vs cachexia. Only genes that are significantly different (adjusted p-value ≤ 0.05) in both groups were plotted.

Expanded View Figure 4: Cachexia and aging have similar effects on MuSC transcriptome

a. Scatter plot comparing LFC of healthy control male MuSCs vs cachectic male MuSCs and the LFC of young male MuSCs and aged male MuSCs. The young and aged MuSC RNA-Seq data is publicly available and was retrieved from GSE171997. Only genes that had an LFC $\geq$ 0.5 in both conditions were plotted. **b.** Scatter plot comparing LFC of healthy control male MuSCs vs cachectic male MuSCs and the LFC of young male MuSCs and aged male MuSCs. Only significant genes were plotted (LFC $\geq$ 0.5 and adjusted p-value $\leq$ 0.05). Bar graphs of the absolute expression (RPM) of **c.** Sparc, **d.** Col3a1, **e.** Ccnd1, **f.** Ccl7, **g.** Ccl11, **h.** RNASE4 between male healthy controls, tumor bearing, young and aged MuSCs.

Expanded View Figure 5: C26 cells reduce muscle stem cell growth and differentiation

a. Representative pictures of EDL myofibers cultured for 72 hours in Unsupplemented Growth Media (15% FBS, 1% P/S, - CEE, - bFGF), Normal Growth Media (15% FBS, 1% P/S, 1% CEE, 5 ng/µL of bFGF) and C26 Conditioned Media (Normal Growth Media cultured for 48 hours with C26 cells). Myofibers were stained for Myogenin. Scale bar = 40 µm. **b.** Quantification of the total number of MuSCs per myofiber, cultured for 72 hours. n = 3 biological replicates. **c.** Quantification of the percentage of Myogenin positive MuSCs per myofiber, cultured for 72 hours. n = 3 biological replicates. Percentage of Myogenin positive primary myoblasts cultured in Unsupplemented, Normal Growth, and C26 Conditioned media for **d.** 12 hours, **e.** 24 hours, and **f.** 36 hours. n = 3 biological replicates. Representative images of primary myoblasts cultured in Unsupplemented Growth Media (20% FBS, 1% P/S), Normal Growth (20% FBS, 1% P/S, 5 ng/µL of bFGF), and C26 Conditioned Media (Normal Growth Media cultured for 48 hours with C26 cells) for **g.** 12 hours, **h.** 24 hours, **i.** and 36 hours. Primary myoblasts were stained for Myogenin. Scale bar = 30 µm. **j.** Bar graph of the protein level of MyoD in primary myoblasts quantified by In Cell Western blot, normalized to control. n=6 replicates per condition. **k.** Bar graph of the protein level of Myogenin in primary myoblasts quantified by In Cell Western blot, normalized to control. n=6 replicates per condition. **l.** Representative image of In Cell Western wells for MyHC, Myog and Myod in control and conditioned media treated conditions. **m.** Bar graph of the protein level of MyHC in 3DM primary myotubes quantified by In Cell Western blot, normalized to control. n=6 replicates per condition. **n.** Representative picture of primary myotubes differentiated for five days, with or without coculture with C26 cells. Cells were stained for Myogenin. Scale bar = 40 µm. **o.** Quantification of the percentage of Myogenin positive nuclei in 5DM myotubes, with or without C26 coculture. n = 3 biological replicates. **p.** Representative pictures of primary myotubes differentiated for 5 days, with or without C26 coculture. Cells were stained for Myosin Heavy Chain. Scale bar = 60 µm. **q.** Quantification of the fusion index of 5DM primary myotubes, with or without C26 coculture. n = 3 biological replicates. **r.** Quantification of the average myotube diameter, defined as the widest region across the myotube, of 5DM primary myotubes with or without C2 coculture. n = 3 biological replicates, 4 fields of view per replicate.

Expanded View 6: Sex of the host does not affect transcriptional adaptation of C26 cancer cells

a. Table of the number of differentially expressed genes between *In vitro* C26 vs *In vivo* in Female, *In vitro* C26 vs *In vivo* in Male, and *In vivo* in Female vs *In vivo* in Male. **b.** Volcano plot comparing gene expression between *In vitro* C26 and *In vivo* in Male. **c.** Heatmap of the differentially expressed (adjusted p-value ≤ 0.1) between *In vitro* C26 vs *In vivo* in Male. **d.** Top ten most significantly enriched Hallmark pathways between *In vitro* C26 vs *In vivo* in Male. Blue bars indicate a pathway is downregulated, orange bars indicate a pathway is upregulated. **e.** Bar plot indicating the absolute expression (RPM) of selected immune cell related genes in *In vitro* C26, *In vivo* in Female, and *In vivo* in Male RNA-Seq samples. **f.** Bar plot of the absolute expression (RPM) of selected Y chromosome genes in Male MuSCs, Female MuSCs, *In vitro* C26, *In vivo* in Female, and *In vivo* in Male RNA-Seq samples. **g.** Heatmap of the Y chromosome gene expression in *In vitro* C26, *In vivo* in Female, and *In vivo* in Male RNA-Seq samples.

Expanded View 7: Cancer patients with high expression of GDF15 and MMP9 have a worse prognosis

a. Expression of MMP9 in C26 cells. **b.** Bar graph of the absolute expression of GDF15 transcript (RPM) in GFP-C26 cells cultured *in vitro* or isolated *in vivo* from male and female tumor bearing mice. **c.** Bar graph of the absolute expression of GDF15 transcript (RPM) in MuSCs freshly isolated from male and female 3-month-old healthy control and tumor bearing mice. **d.** Kaplan Meier curve of colon adenocarcinoma patients with high and low expression of GDF15 in the tumor. GDF15 high n = 22; GDF15 low n = 14. **e.** Kaplan Meier curve of colon adenocarcinoma patients with high and low expression of MMP9 in the tumor. MMP9 high n = 16; MMP9 low n = 20. **f.** Kaplan Meier survival curve of pancreatic adenocarcinoma patients with high and low expression of GDF15 in the tumor. GDF15 high n = 31; GDF15 low n = 23. Data was retrieved from TCGA and only patients that did not undergo chemotherapy or surgery were selected. **g.** Kaplan Meier survival curve of pancreatic adenocarcinoma patients with high and low expression of MMP9 in the tumor. MMP9 high n = 30; MMP9 low n = 24. Data was retrieved from TCGA and only patients that did not undergo chemotherapy or surgery were selected.

Expanded View 8: MMP9 treatment increases SNAI1 expression in primary myoblasts

a. Bar graph of the relative expression of SNAI1 in 3DM primary myotubes cultured in normal and C26 conditioned media. n=4. **b.** Representative images of primary myoblasts treated with MMP9 and stained for MyoD1, SNAI1, and Myogenin. Scale bar = 30 um. n = 3 biological replicates. **c.** Percentage of the high SNAI1 expressing primary myoblasts treated with MMP9. **d.** Percentage of Myogenin positive primary myoblast treated with MMP9. **e.** Representative image of isolated EDL myofibers cultured for 36 hours before being treated with MMP9 for 1 hour. n = 3 biological replicates. Myofibers were stained with MyoD and phosphor-SMAD3. **f.** Percentage of high phosphor-SMAD3 expressing MuSCs per myofiber. **g.** Representative image of isolated EDL myofibers cultured and treated with GDF15 for 60 hours and stained for MyoD and Myogenin. n = 3 biological replicates. **h.** quantification of the number of MuSCs per myofiber after 60 hours in culture. **i.** Quantification of the percentage of Myogenin positive MuSCs per myofiber after 60 hours in culture. **j.** Quantification of the percentage of Myogenin expressing MuSCs per EDL myofiber from myofibers cultured for 72 hours in unsupplemented, normal growth and GDF15 treated conditions. **k.** Quantification of the percentage of high SNAI1 expressing primary myoblasts that were cultured for 24 hours in unsupplemented, normal growth and GDF15 treated conditions. **l.** Quantification of the percentage of Myogenin expressing primary myoblasts that were cultured for 24 hours in unsupplemented, normal growth and GDF15 treated conditions. **m.** Representative pictures of primary myoblasts cultured for 24 hours in unsupplemented (20% FBS, 1% P/S), normal growth (20% FBS, 1% P/S, 5 ng/μL bFGF), or GDF15 treated (20% FBS, 1%P/S, 500 ng/μL GDF15) media. The GDF15 was added every 12 hours. Primary myoblasts were stained for SNAI1 and Myogenin. n = 3 biological replicates. Scale bar = 50 μm.

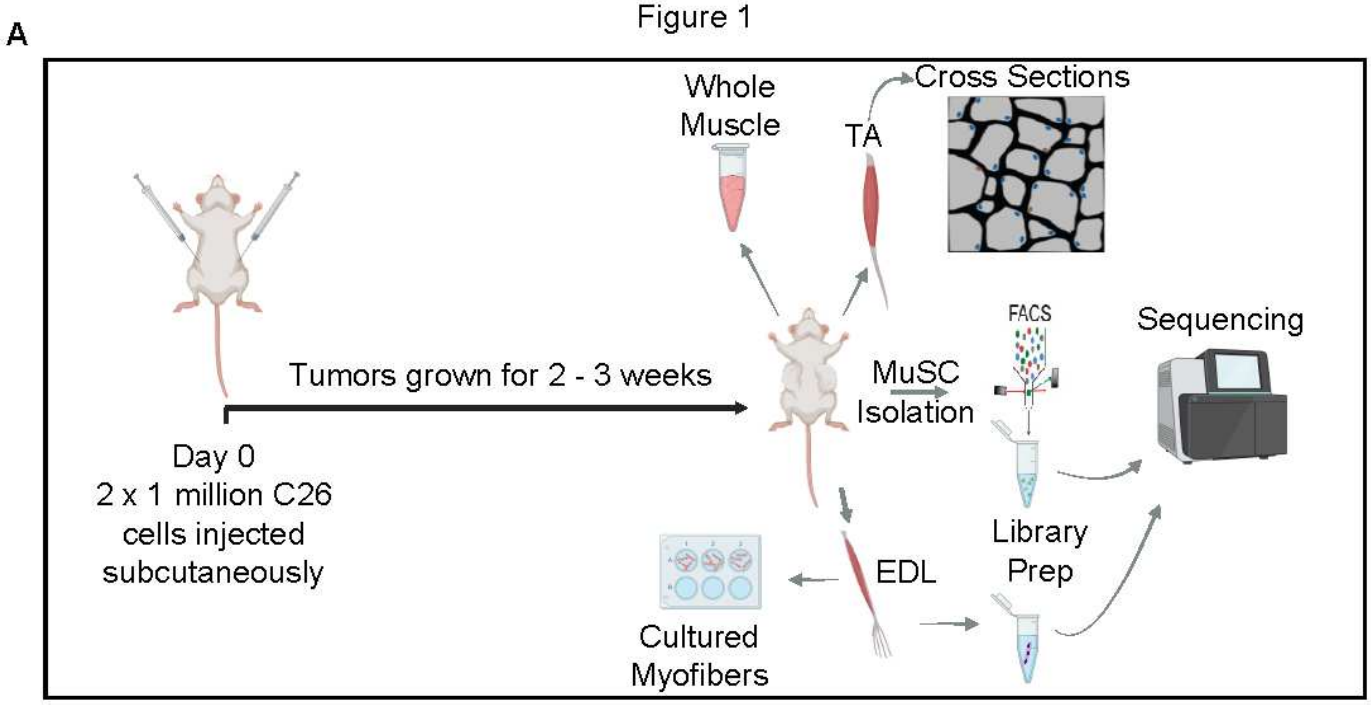
Expanded View 9: Tumor specific knockout of GDF15 does not prevent cachexia

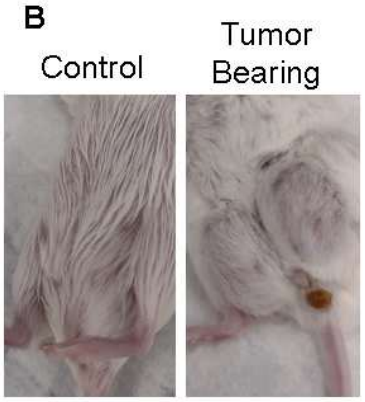
a. Bar graph of the tumor free mass of female balb/c mice that are either healthy controls, mice injected with Crispr Control C26 cancer cells, or mice injected with Crispr GDF15 KO C26 cancer cells. All tumor bearing mice were injected with C26 cells at 3 months of age. Tumor free mass was assessed when mice reached endpoint, healthy controls were collected at the end of the experiment. n = 3 healthy controls, 6 Crispr Controls and 8 GDF15 KO. **b.** Bar graph of the mass of the tumors isolated from the Crispr Control and GDF15 KO tumor bearing mice. n = 6 Crispr Controls and 8 GDF15 KO. **c.** Bar graphs of the mass of the tibialis anterior (TA) isolated from healthy controls, Crispr Control and GDF15 KO tumor bearing mice. n = 6 TAs from healthy controls, 12 TAs from Crispr Controls, and 16 TAs from GDF15 KO. **d.** Quantification of the cross-sectional area (CSA) of myofibers in the TA isolated from Healthy Controls, Crispr Controls and GDF15 KO tumor bearing mice. Data is presented as percentage of myofibers that are within the marked size range. n = 3 healthy controls, 6 Crispr Controls and 6 GDF15 KO tumor bearing mice. **e.** Representative picture of the CSA of myofibers from the TA of Healthy Control, Crispr Control, and GDF15 KO tumor bearing mice. Cross sections were stained for Laminin. Scale bar = 80 μm. **f.** Quantification of fat mass as a percentage of whole body mass, measured by EchoMRI 19 days post tumor cell injection. **g.** Quantification of lean mass as a percentage of whole body mass, measured by EchoMRI 19 days post tumor cell injection. **h.** Quantification of the level of serum GDF15, measured by ELISA, from Crispr Control and GDF15 KO tumor bearing mice. Blood was collected 14 days post tumor injection. n = 4 mice. **i.** Daily food intake of Cripsr Control and GDF15 KO tumor bearing mice. Food intake was measured using a Comprehensive Lab Animal Monitoring System (CLAMS) for 3 days in the second week post tumor injection. n = 5 mice. **j.** Daily Respiratory Exchange Rate (RER) of Cripsr Control and GDF15 KO tumor bearing mice. RER was measured using a CLAMS for 3 days in the second week post tumor injection. n = 5 mice. **k.** Daily food intake of Cripsr Control and GDF15 KO tumor bearing mice. Food intake was measured using a Comprehensive Lab Animal Monitoring System (CLAMS) for 3 days in the third week post tumor injection. n = 5 mice. **l.** Daily Respiratory Exchange Rate (RER) of Cripsr Control and GDF15 KO tumor bearing mice. RER was measured using a CLAMS for 3 days in the third week post tumor injection. n = 5 mice.

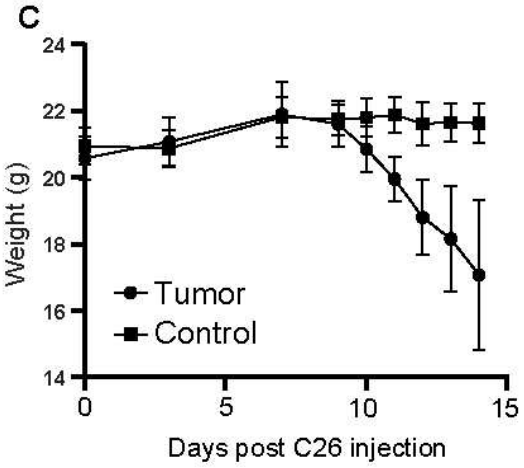
Expanded View 10: Primary myoblasts cocultured with GDF15 KO C26 cells show no phenotypic improvement

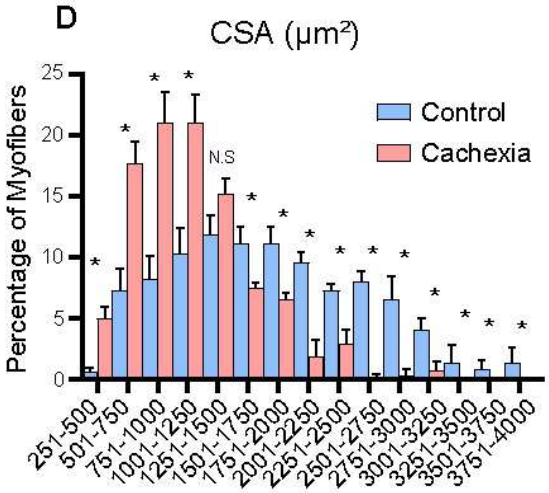
a. Representative images of a 12-hour EDU incorporation assay performed on Crispr Control and GDF15 KO C26 cells. **b.** Quantification of the percentage of EDU positive C26 hours after 12-hour EDU incorporation. **c.** Representative images of a 12-hour EDU incorporation assay performed on primary myoblasts that were not cocultured, or cocultured with Crispr Control or GDF15 KO C26 cells. **d.** Quantification of the percentage of EDU positive primary myoblasts after a 12-hour EDU incorporation. **e.** Representative images of primary myotubes that were differentiated for 5 days and were either not cocultured, or cocultured with Crispr Control or GDF15 KO C26 cells. **f.** Bar graph of the fusion index of primary myotubes that were differentiated for 5 days and were either not cocultured, or cocultured with Crispr Control or GDF15 KO C26 cells. **g.** Representative images of isolated EDL myofibers that were either not cocultured, or cocultured with Crispr Control or GDF15 KO C26 cells for 72 hours. Myofibers were stained for MyoD and Myogenin. Scale bar = 40 μm. n = 3 biological replicates. **h.** Quantification of the number of MuSCs per myofiber on isolated EDL myofibers cultured for 72 hours in growth media, or cocultured with Crispr Control or GDF15 KO C26 cells. **i.** Percentage of Myogenin positive MuSCs per myofiber in isolated EDL myofibers cultured for 72 hours in growth media, or cocultured with Crispr Control or GDF15 KO C26 cells.

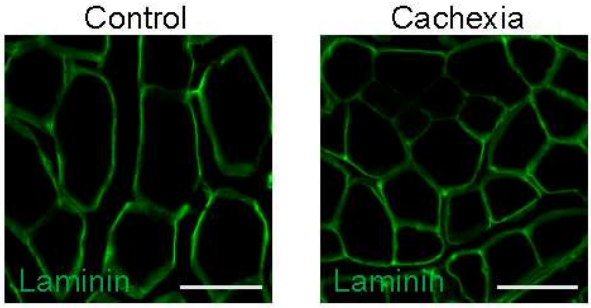
Figure 1

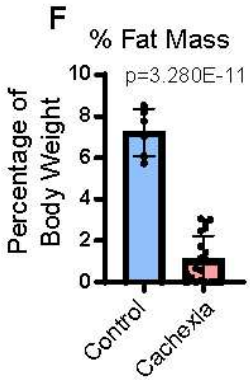

A
Whole Muscle
TA
Cross Sections
FACS
Sequencing
Tumors grown for 2 - 3 weeks
MuSC Isolation
Day 0
2 x 1 million C26 cells injected subcutaneously
Library Prep
EDL
Cultured Myofibers

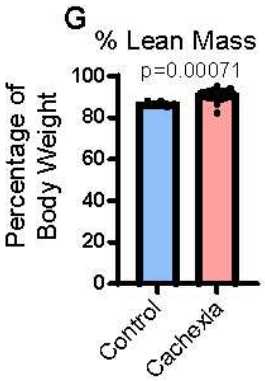

B
Control
Tumor Bearing

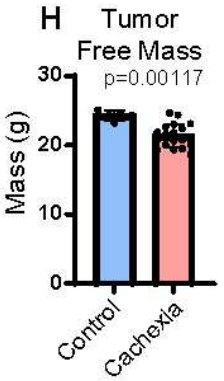

C
Weight (g)
Tumor
Control
Days post C26 injection

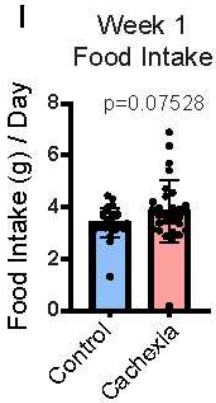

D
CSA (μm²)
Percentage of Myofibers
Control
Cachexia
N.S
251-500
501-750
751-1000
1001-1250
1251-1500
1501-1750
1751-2000
2001-2250
2251-2500
2501-2750
2751-3000
3001-3250
3251-3500
3501-3750
3751-4000

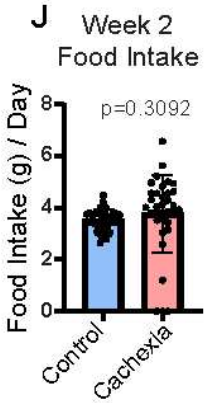

E
Control
Cachexia
Laminin
Laminin

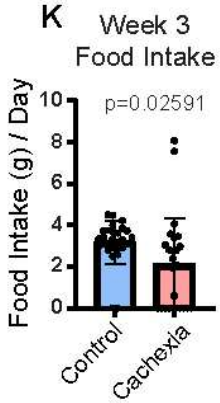

F
% Fat Mass
p=3.280E-11
Percentage of Body Weight
Control
Cachexia

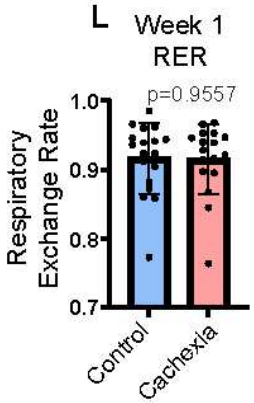

G
% Lean Mass
p=0.00071
Percentage of Body Weight
Control
Cachexia

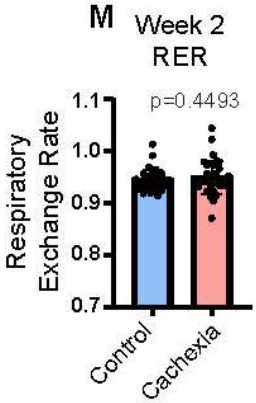

H
Tumor Free Mass
p=0.00117
Mass (g)
Control
Cachexia


I
Week 1 Food Intake
p=0.07528
Food Intake (g) / Day
Control
Cachexia


J
Week 2 Food Intake
p=0.3092
Food Intake (g) / Day
Control
Cachexia


K
Week 3 Food Intake
p=0.02591
Food Intake (g) / Day
Control
Cachexia


L
Week 1 RER
p=0.9557
Respiratory Exchange Rate
Control
Cachexia


M
Week 2 RER
p=0.4493
Respiratory Exchange Rate
Control
Cachexia

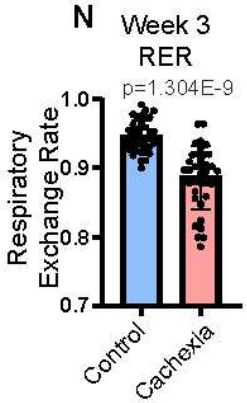

N
Week 3 RER
p=1.304E-9
Respiratory Exchange Rate
Control
Cachexia

Figure 2

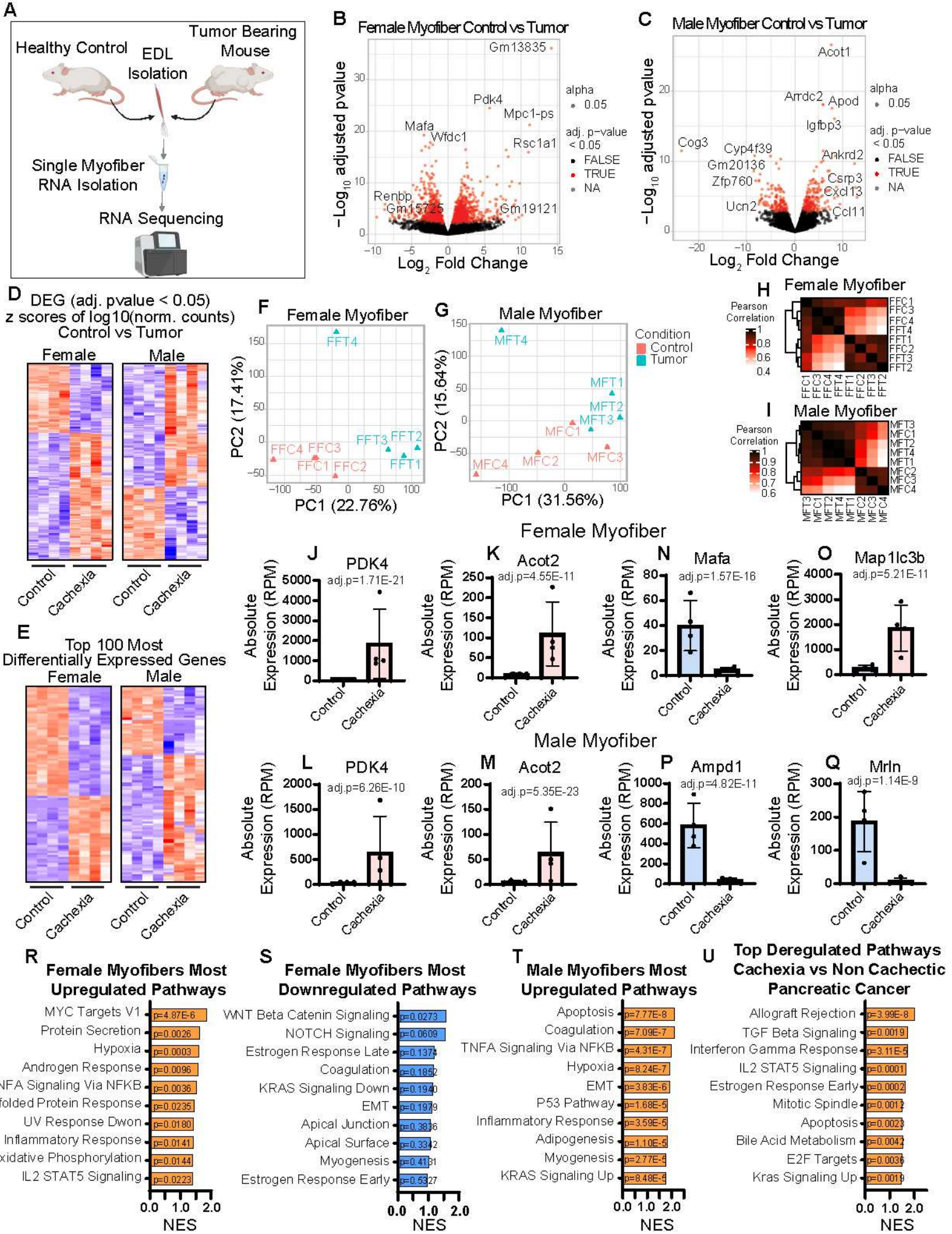

A
Healthy Control
EDL Isolation
Tumor Bearing Mouse
Single Myofiber RNA Isolation
RNA Sequencing
B
Female Myofiber Control vs Tumor
−Log10 adjusted pvalue
Log2 Fold Change
alpha
0.05
adj. p−value < 0.05
FALSE
TRUE
NA
Gm13835
Pdk4
Mpc1-ps
Mafa
Wfdc1
Rsc1a1
Renbp
Gm15725
Gm19121
C
Male Myofiber Control vs Tumor
Acot1
Arrdc2
Apod
Igfbp3
Cog3
Cyp4f39
Gm20136
Zfp760
Ankrd2
Csrp3
Cxcl13
Ucn2
Ccl11
D
DEG (adj. pvalue < 0.05)
z scores of log10(norm. counts)
Control vs Tumor
Female
Male
Control
Cachexia
E
Top 100 Most Differentially Expressed Genes
F
Female Myofiber
PC2 (17.41%)
PC1 (22.76%)
FFT4
FFT3
FFT2
FFC4
FFC3
FFC1
FFC2
FFT1
G
Male Myofiber
PC2 (15.64%)
PC1 (31.56%)
Condition
Control
Tumor
MFT4
MFT1
MFT2
MFT3
MFC1
MFC4
MFC2
MFC3
H
Female Myofiber
Pearson Correlation
I
Male Myofiber
J
PDK4
adj.p=1.71E-21
K
Acot2
adj.p=4.55E-11
N
Mafa
adj.p=1.57E-16
O
Map1lc3b
adj.p=5.21E-11
Absolute Expression (RPM)
L
PDK4
adj.p=6.26E-10
M
Acot2
adj.p=5.35E-23
P
Ampd1
adj.p=4.82E-11
Q
Mrln
adj.p=1.14E-9
R
Female Myofibers Most Upregulated Pathways
MYC Targets V1
Protein Secretion
Hypoxia
Androgen Response
TNFA Signaling Via NFKB
Unfolded Protein Response
UV Response Dwon
Inflammatory Response
Oxidative Phosphorylation
IL2 STAT5 Signaling
NES
S
Female Myofibers Most Downregulated Pathways
WNT Beta Catenin Signaling
NOTCH Signaling
Estrogen Response Late
Coagulation
KRAS Signaling Down
EMT
Apical Junction
Apical Surface
Myogenesis
Estrogen Response Early
T
Male Myofibers Most Upregulated Pathways
Apoptosis
Coagulation
TNFA Signaling Via NFKB
Hypoxia
EMT
P53 Pathway
Inflammatory Response
Adipogenesis
Myogenesis
KRAS Signaling Up
U
Top Deregulated Pathways Cachexia vs Non Cachectic Pancreatic Cancer
Allograft Rejection
TGF Beta Signaling
Interferon Gamma Response
IL2 STAT5 Signaling
Estrogen Response Early
Mitotic Spindle
Apoptosis
Bile Acid Metabolism
E2F Targets
Kras Signaling Up

Figure 3

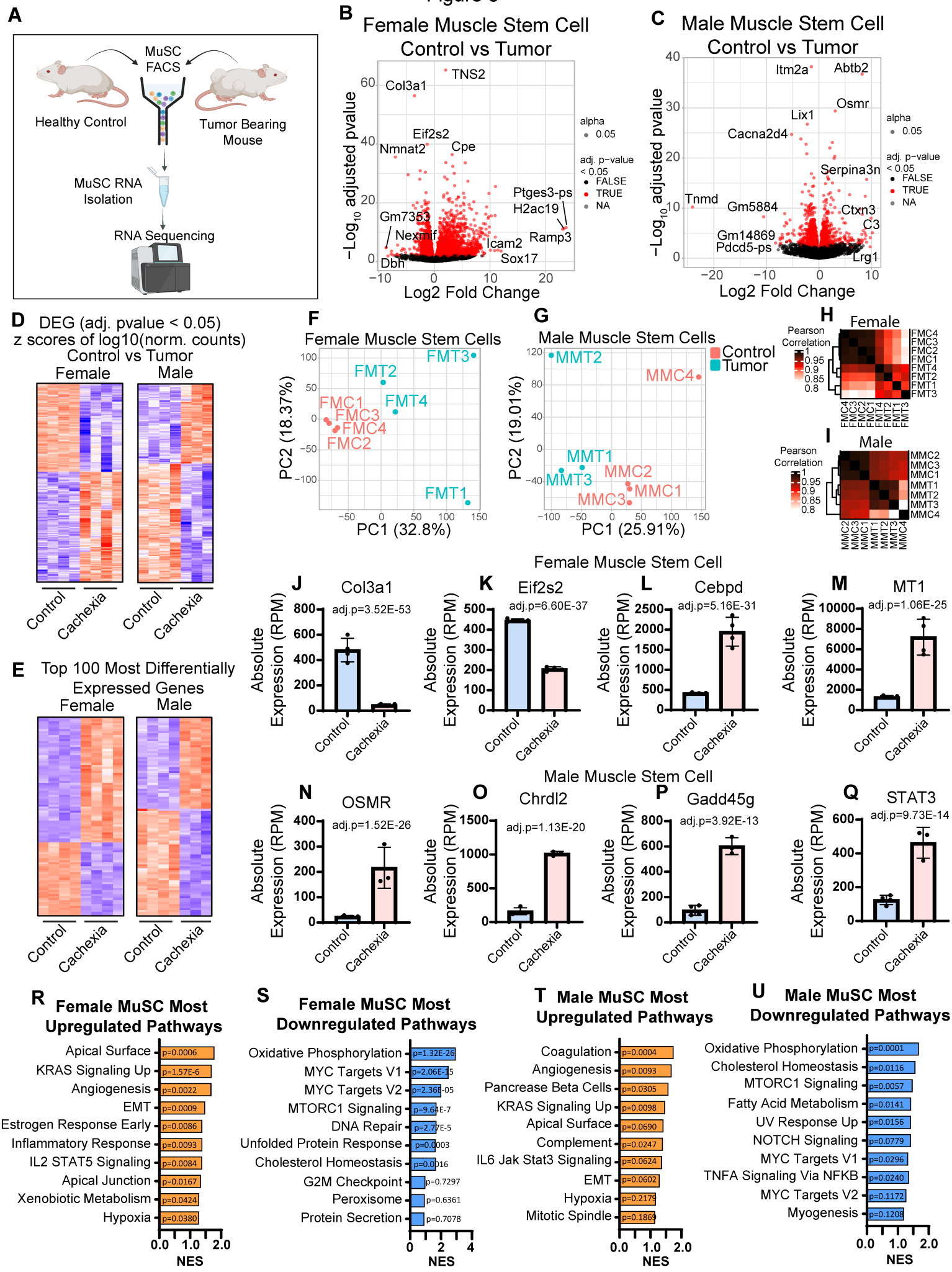
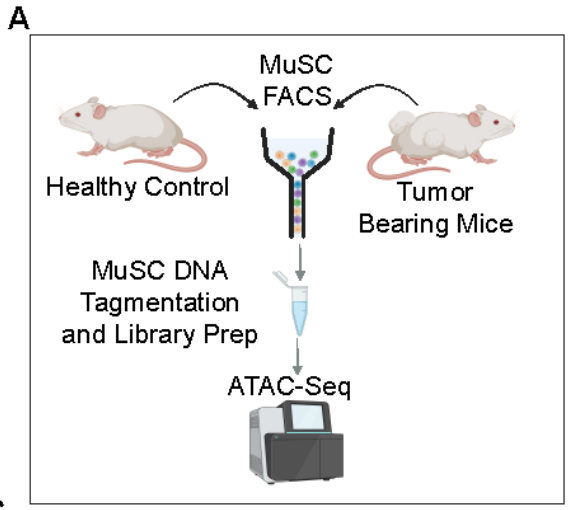
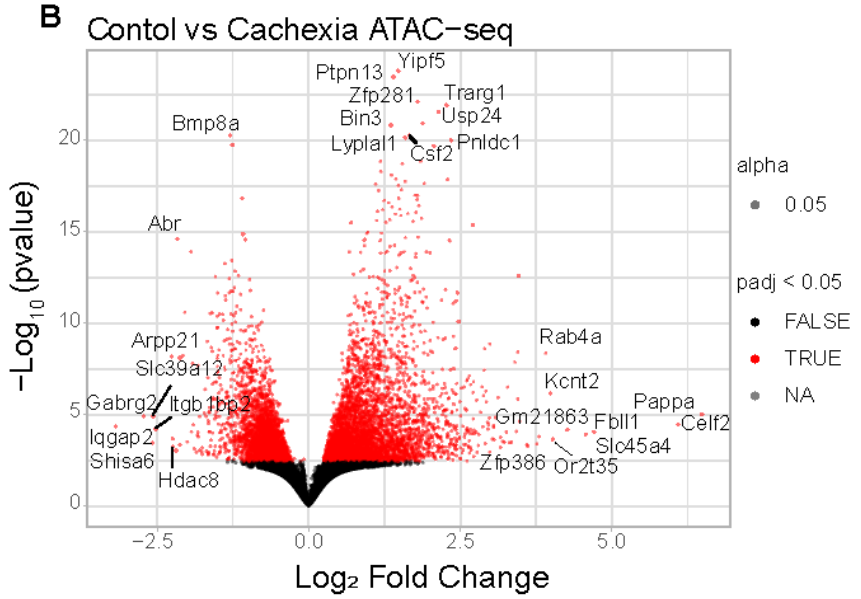
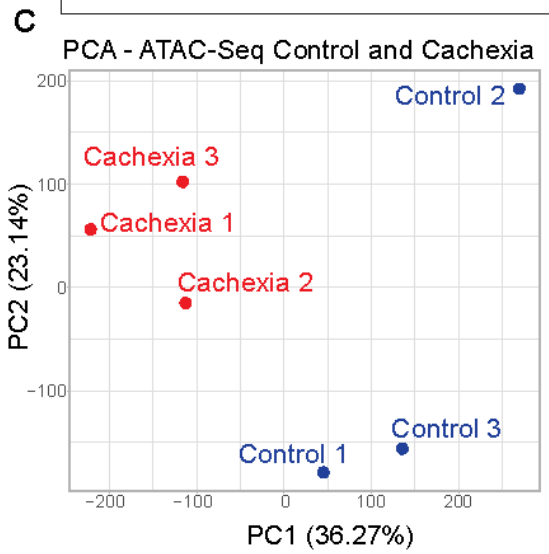
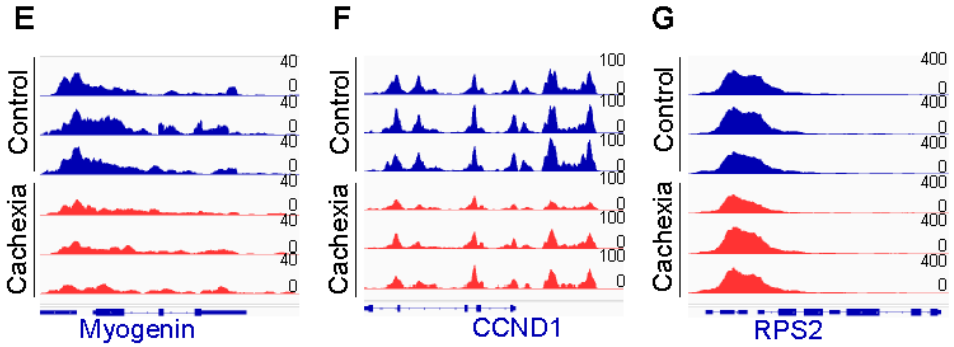

A
MuSC FACS
Healthy Control
Tumor Bearing Mouse
MuSC RNA Isolation
RNA Sequencing
B
Female Muscle Stem Cell Control vs Tumor
−Log10 adjusted pvalue
Log2 Fold Change
TNS2
Col3a1
Eif2s2
Nmnat2
Cpe
Ptges3-ps
H2ac19
Gm7353
Nexmif
Icam2
Ramp3
Dbn
Sox17
alpha 0.05
adj. p−value < 0.05 FALSE TRUE NA
C
Male Muscle Stem Cell Control vs Tumor
Itm2a
Abtb2
Osmr
Lix1
Cacna2d4
Serpina3n
Tnmd
Gm5884
Ctxn3
C3
Gm14869
Pdcd5-ps
Lrg1
D
DEG (adj. pvalue < 0.05)
z scores of log10(norm. counts)
Control vs Tumor
Female
Male
Control
Cachexia
E
Top 100 Most Differentially Expressed Genes
F
Female Muscle Stem Cells
PC2 (18.37%)
PC1 (32.8%)
FMT3
FMT2
FMC1
FMT4
FMC3
FMC4
FMC2
FMT1
G
Male Muscle Stem Cells
PC2 (19.01%)
PC1 (25.91%)
Control
Tumor
MMT2
MMC4
MMT1
MMT3
MMC2
MMC3
MMC1
H
Female
Pearson Correlation
I
Male
J
Col3a1
adj.p=3.52E-53
K
Eif2s2
adj.p=6.60E-37
L
Cebpd
adj.p=5.16E-31
M
MT1
adj.p=1.06E-25
Female Muscle Stem Cell
Absolute Expression (RPM)
N
OSMR
adj.p=1.52E-26
O
Chrdl2
adj.p=1.13E-20
P
Gadd45g
adj.p=3.92E-13
Q
STAT3
adj.p=9.73E-14
Male Muscle Stem Cell
R
Female MuSC Most Upregulated Pathways
Apical Surface p=0.0006
KRAS Signaling Up p=1.57E-6
Angiogenesis p=0.0022
EMT p=0.0009
Estrogen Response Early p=0.0086
Inflammatory Response p=0.0093
IL2 STAT5 Signaling p=0.0084
Apical Junction p=0.0167
Xenobiotic Metabolism p=0.0424
Hypoxia p=0.0380
NES
S
Female MuSC Most Downregulated Pathways
Oxidative Phosphorylation p=1.32E-26
MYC Targets V1 p=2.06E-15
MYC Targets V2 p=2.36E-05
MTORC1 Signaling p=9.64E-7
DNA Repair p=2.77E-5
Unfolded Protein Response p=0.0003
Cholesterol Homeostasis p=0.0016
G2M Checkpoint p=0.7297
Peroxisome p=0.6361
Protein Secretion p=0.7078
NES
T
Male MuSC Most Upregulated Pathways
Coagulation p=0.0004
Angiogenesis p=0.0093
Pancrease Beta Cells p=0.0305
KRAS Signaling Up p=0.0098
Apical Surface p=0.0690
Complement p=0.0247
IL6 Jak Stat3 Signaling p=0.0624
EMT p=0.0602
Hypoxia p=0.2179
Mitotic Spindle p=0.1869
NES
U
Male MuSC Most Downregulated Pathways
Oxidative Phosphorylation p=0.0001
Cholesterol Homeostasis p=0.0116
MTORC1 Signaling p=0.0057
Fatty Acid Metabolism p=0.0141
UV Response Up p=0.0156
NOTCH Signaling p=0.0779
MYC Targets V1 p=0.0296
TNFA Signaling Via NFKB p=0.0240
MYC Targets V2 p=0.1172
Myogenesis p=0.1208
NES

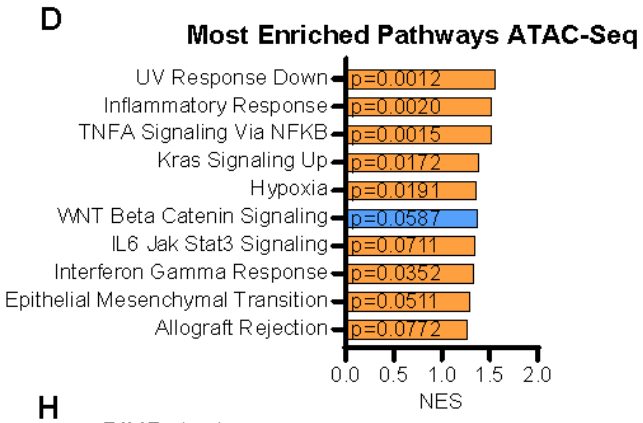
Figure 4

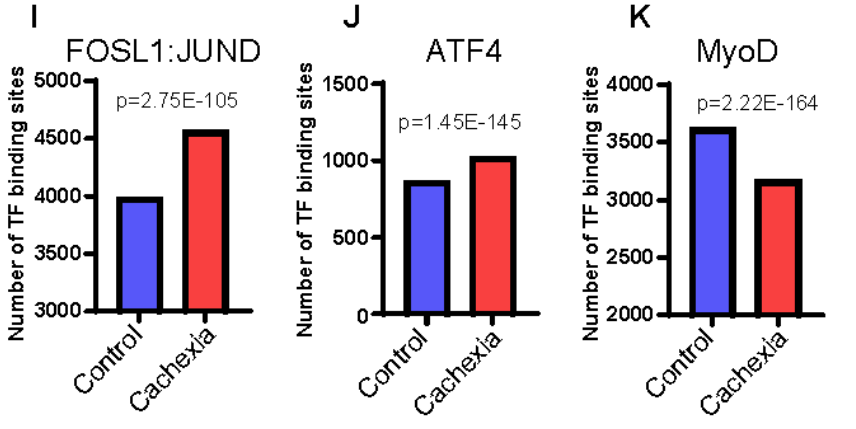

A
MuSC
FACS
Healthy Control
Tumor
Bearing Mice
MuSC DNA
Tagmentation
and Library Prep
ATAC-Seq

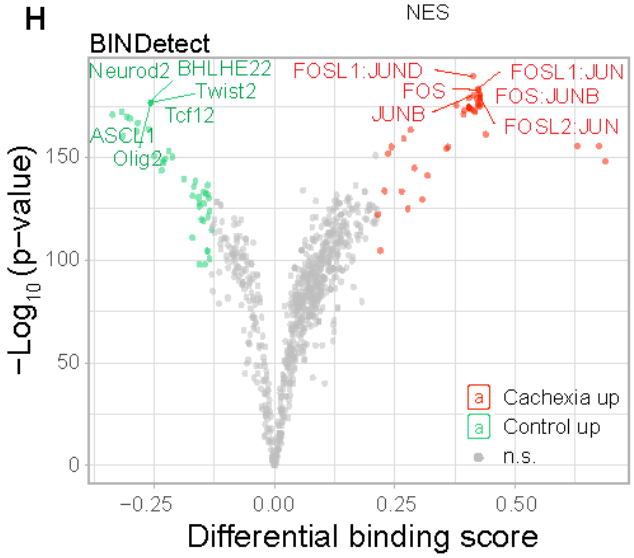

B
Contol vs Cachexia ATAC−seq
Ptpn13
Yipf5
Zfp281
Trarg1
Bin3
Usp24
Bmp8a
Lyplal1
Pnldc1
Csf2
Abr
Arpp21
Slc39a12
Rab4a
Kcnt2
Gabrg2
Itgb1bp2
Pappa
Gm21863
Fbll1
Celf2
Iqgap2
Slc45a4
Shisa6
Zfp386
Or2t35
Hdac8
−Log10 (pvalue)
Log2 Fold Change
alpha
0.05
padj < 0.05
FALSE
TRUE
NA


C
PCA - ATAC-Seq Control and Cachexia
Control 2
Cachexia 3
Cachexia 1
Cachexia 2
Control 3
Control 1
PC2 (23.14%)
PC1 (36.27%)


E
F
G
Control
Cachexia
Myogenin
CCND1
RPS2


D
Most Enriched Pathways ATAC-Seq
UV Response Down
Inflammatory Response
TNFA Signaling Via NFKB
Kras Signaling Up
Hypoxia
WNT Beta Catenin Signaling
IL6 Jak Stat3 Signaling
Interferon Gamma Response
Epithelial Mesenchymal Transition
Allograft Rejection
p=0.0012
p=0.0020
p=0.0015
p=0.0172
p=0.0191
p=0.0587
p=0.0711
p=0.0352
p=0.0511
p=0.0772
NES


I
FOSL1:JUND
p=2.75E-105
J
ATF4
p=1.45E-145
K
MyoD
p=2.22E-164
Number of TF binding sites
Control
Cachexia


H
BINDetect
Neurod2 BHLHE22
Twist2
Tcf12
ASCL1
Olig2
FOSL1:JUND
FOS
JUNB
FOSL1:JUN
FOS:JUNB
FOSL2:JUN
Cachexia up
Control up
n.s.
−Log10 (p−value)
Differential binding score

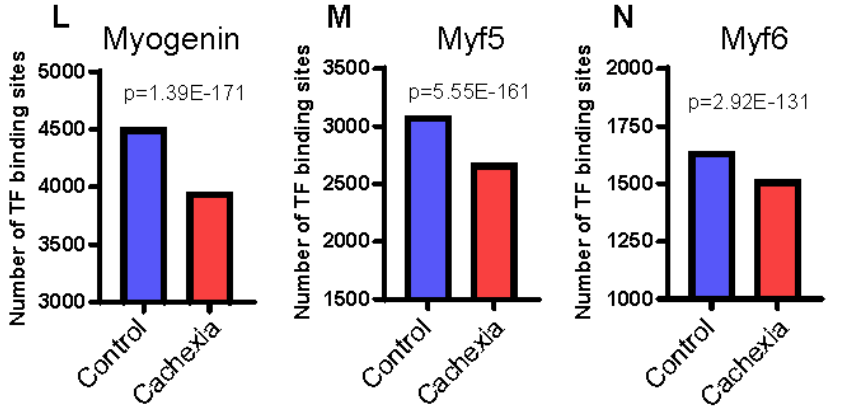

L
Myogenin
p=1.39E-171
M
Myf5
p=5.55E-161
N
Myf6
p=2.92E-131
Number of TF binding sites
Control
Cachexia

Figure 5

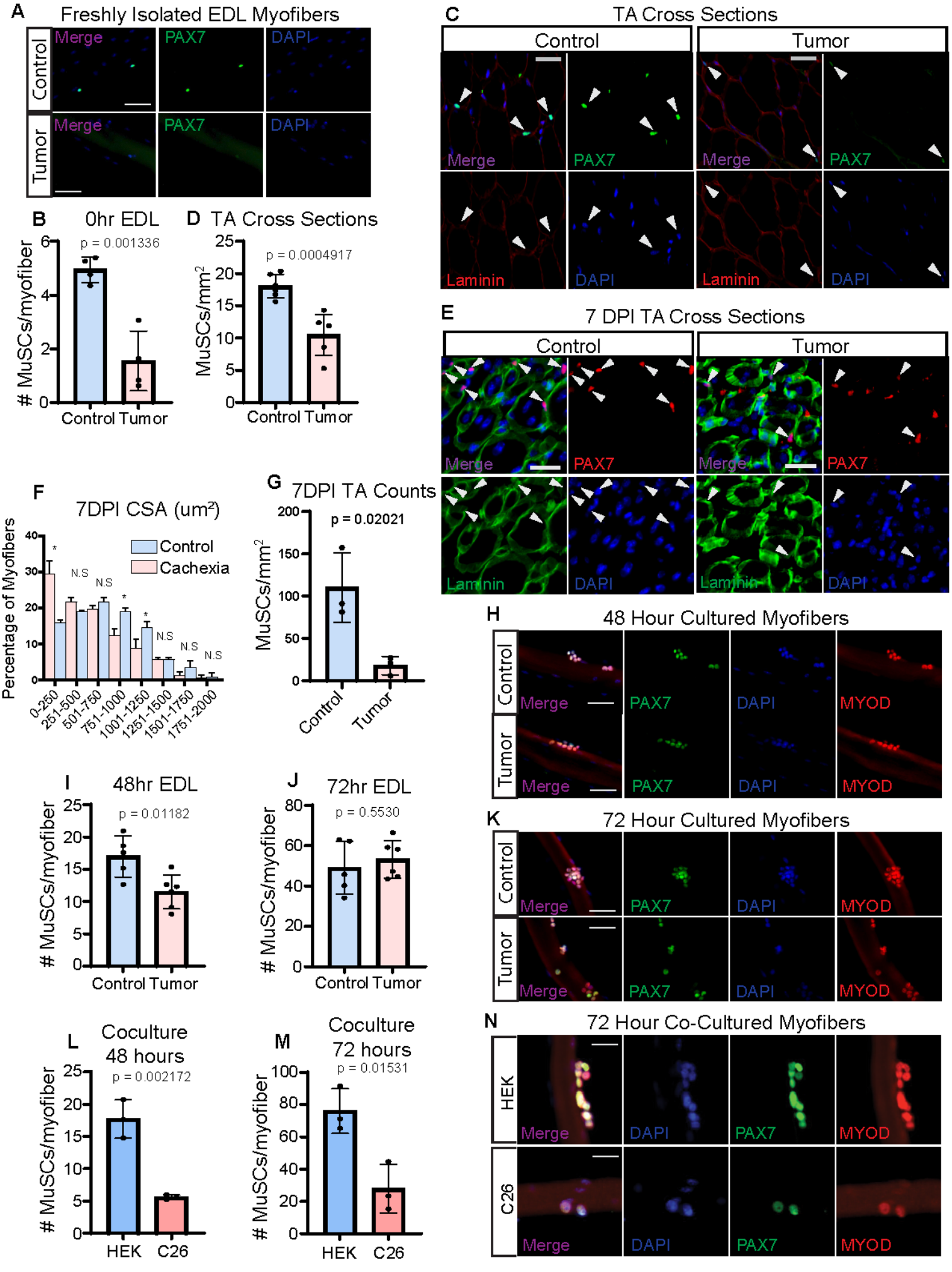

A
Freshly Isolated EDL Myofibers
Control
Tumor
Merge
PAX7
DAPI
B
0hr EDL
p = 0.001336
# MuSCs/myofiber
Control Tumor
D
TA Cross Sections
p = 0.0004917
MuSCs/mm2
Control Tumor
C
TA Cross Sections
Control
Tumor
Merge
PAX7
Laminin
DAPI
E
7 DPI TA Cross Sections
Control
Tumor
Merge
PAX7
Laminin
DAPI
F
7DPI CSA (um2)
Percentage of Myofibers
Control
Cachexia
N.S
0-250
251-500
501-750
751-1000
1001-1250
1251-1500
1501-1750
1751-2000
G
7DPI TA Counts
p = 0.02021
MuSCs/mm2
Control
Tumor
H
48 Hour Cultured Myofibers
Control
Tumor
Merge
PAX7
DAPI
MYOD
I
48hr EDL
p = 0.01182
# MuSCs/myofiber
Control Tumor
J
72hr EDL
p = 0.5530
# MuSCs/myofiber
Control Tumor
K
72 Hour Cultured Myofibers
Control
Tumor
Merge
PAX7
DAPI
MYOD
L
Coculture
48 hours
p = 0.002172
# MuSCs/myofiber
HEK C26
M
Coculture
72 hours
p = 0.01531
# MuSCs/myofiber
HEK C26
N
72 Hour Co-Cultured Myofibers
HEK
C26
Merge
DAPI
PAX7
MYOD

Figure 6

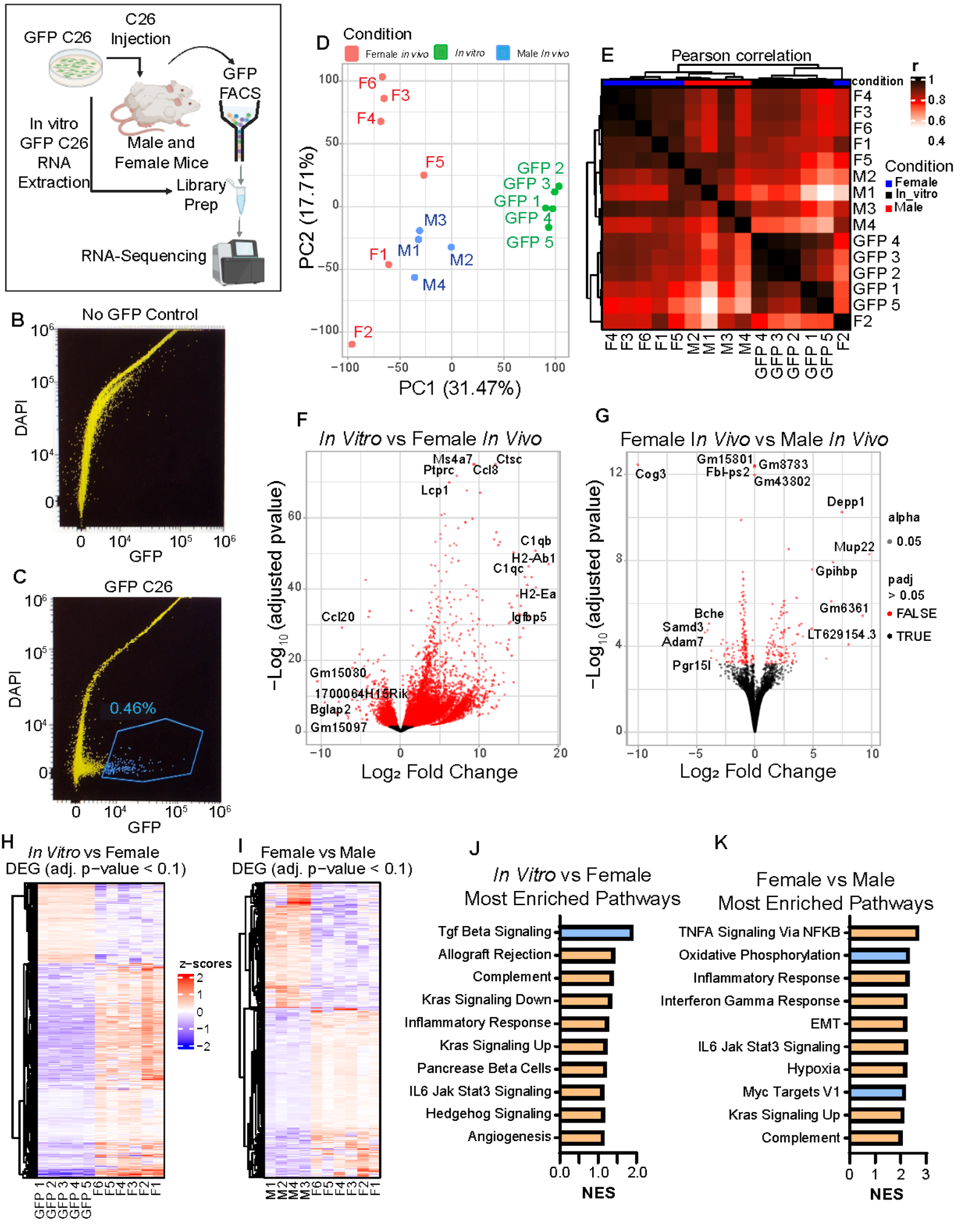

A
GFP C26
C26 Injection
GFP FACS
In vitro GFP C26 RNA Extraction
Male and Female Mice
Library Prep
RNA-Sequencing
B
No GFP Control
DAPI
GFP
C
GFP C26
0.46%
D
Condition
Female In vivo
In vitro
Male In vivo
PC2 (17.71%)
PC1 (31.47%)
E
Pearson correlation
condition
r
Condition
Female
In_vitro
Male
F
In Vitro vs Female In Vivo
−Log10 (adjusted pvalue)
Log2 Fold Change
G
Female In Vivo vs Male In Vivo
alpha
padj
FALSE
TRUE
H
In Vitro vs Female
DEG (adj. p−value < 0.1)
z−scores
I
Female vs Male
DEG (adj. p−value < 0.1)
J
In Vitro vs Female
Most Enriched Pathways
NES
K
Female vs Male
Most Enriched Pathways
NES

Figure 7

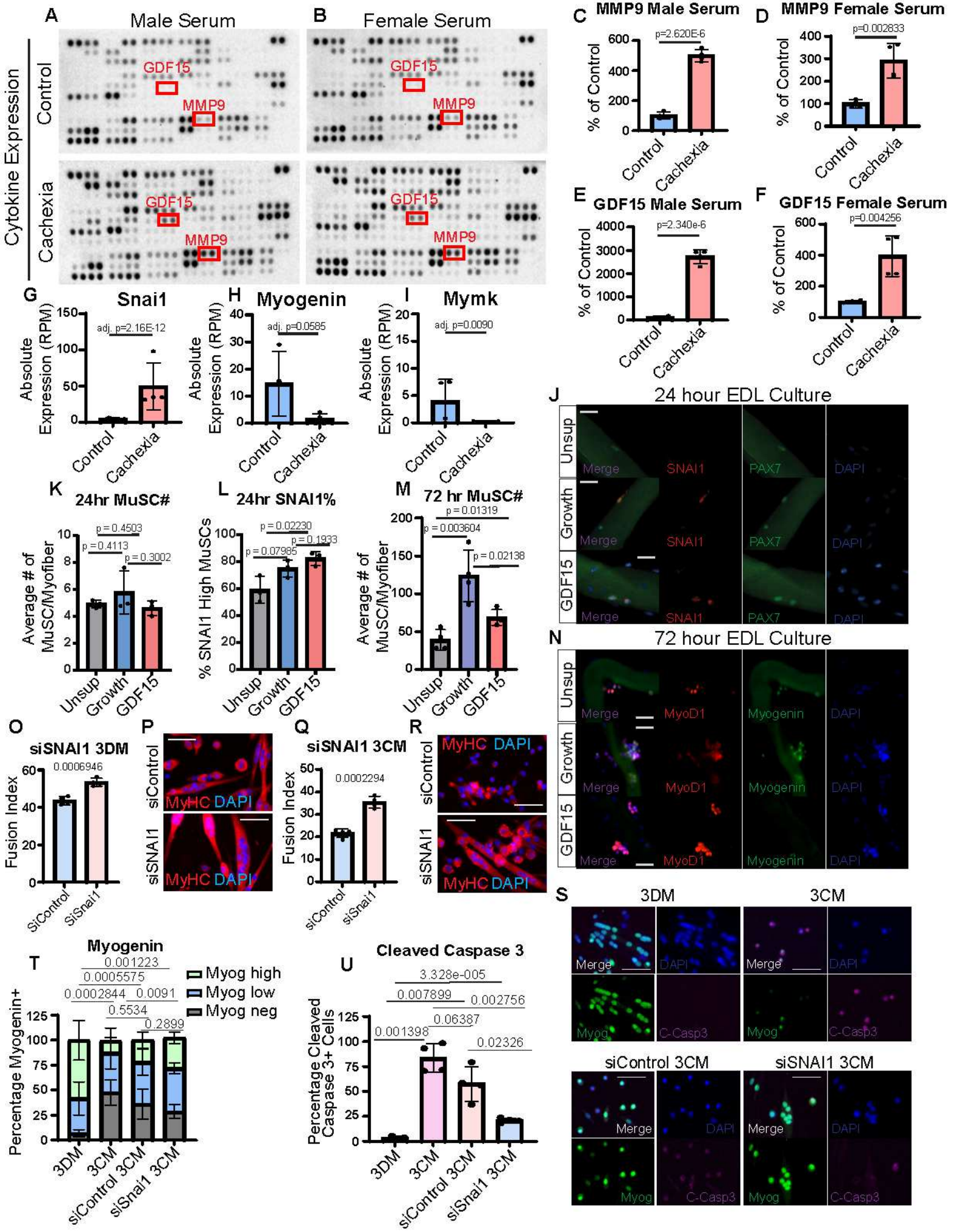

A
Male Serum
B
Female Serum
Cytokine Expression
Control
Cachexia
GDF15
MMP9
C
MMP9 Male Serum
p=2.620E-6
% of Control
D
MMP9 Female Serum
p=0.002833
E
GDF15 Male Serum
p=2.340e-6
F
GDF15 Female Serum
p=0.004256
Control
Cachexia
G
Snai1
adj. p=2.16E-12
H
Myogenin
adj. p=0.0585
I
Mymk
adj. p=0.0090
Absolute Expression (RPM)
J
24 hour EDL Culture
Unsup
Growth
GDF15
Merge
SNAI1
PAX7
DAPI
K
24hr MuSC#
p = 0.4503
p = 0.4113
p = 0.3002
Average # of MuSC/Myofiber
L
24hr SNAI1%
p = 0.02230
p = 0.1933
p = 0.07985
% SNAI1 High MuSCs
M
72 hr MuSC#
p = 0.01319
p = 0.003604
p = 0.02138
N
72 hour EDL Culture
MyoD1
Myogenin
O
siSNAI1 3DM
0.0006946
Fusion Index
SiControl
SiSnai1
P
siControl
siSNAI1
MyHC DAPI
Q
siSNAI1 3CM
0.0002294
R
S
3DM
3CM
siControl 3CM
siSNAI1 3CM
Myog
C-Casp3
T
Myogenin
0.001223
0.0005575
0.0002844
0.0091
0.5534
0.2899
Myog high
Myog low
Myog neg
Percentage Myogenin+
3DM
3CM
siControl 3CM
siSnai1 3CM
U
Cleaved Caspase 3
3.328e-005
0.007899
0.002756
0.06387
0.001398
0.02326
Percentage Cleaved Caspase 3+ Cells

Figure 8

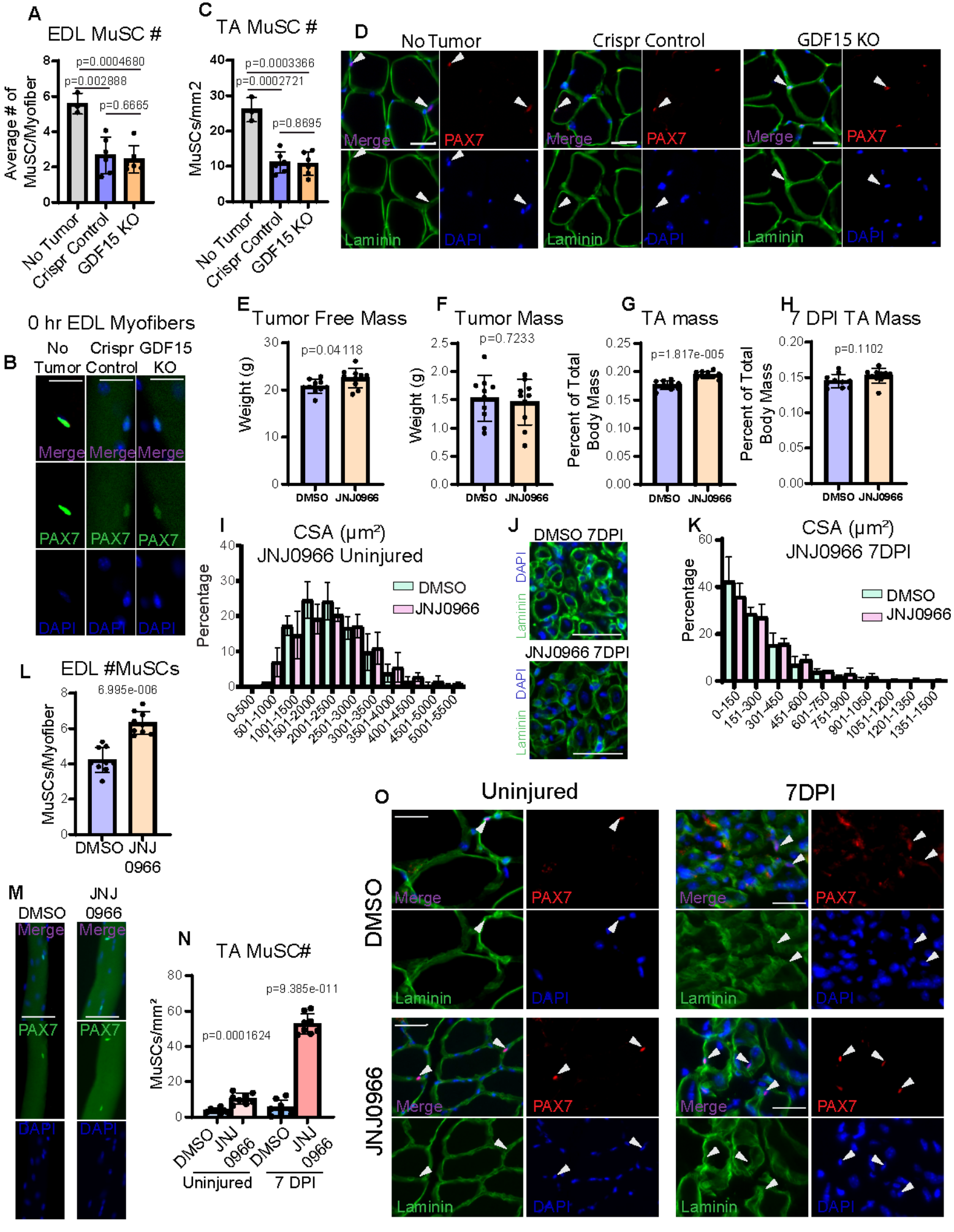
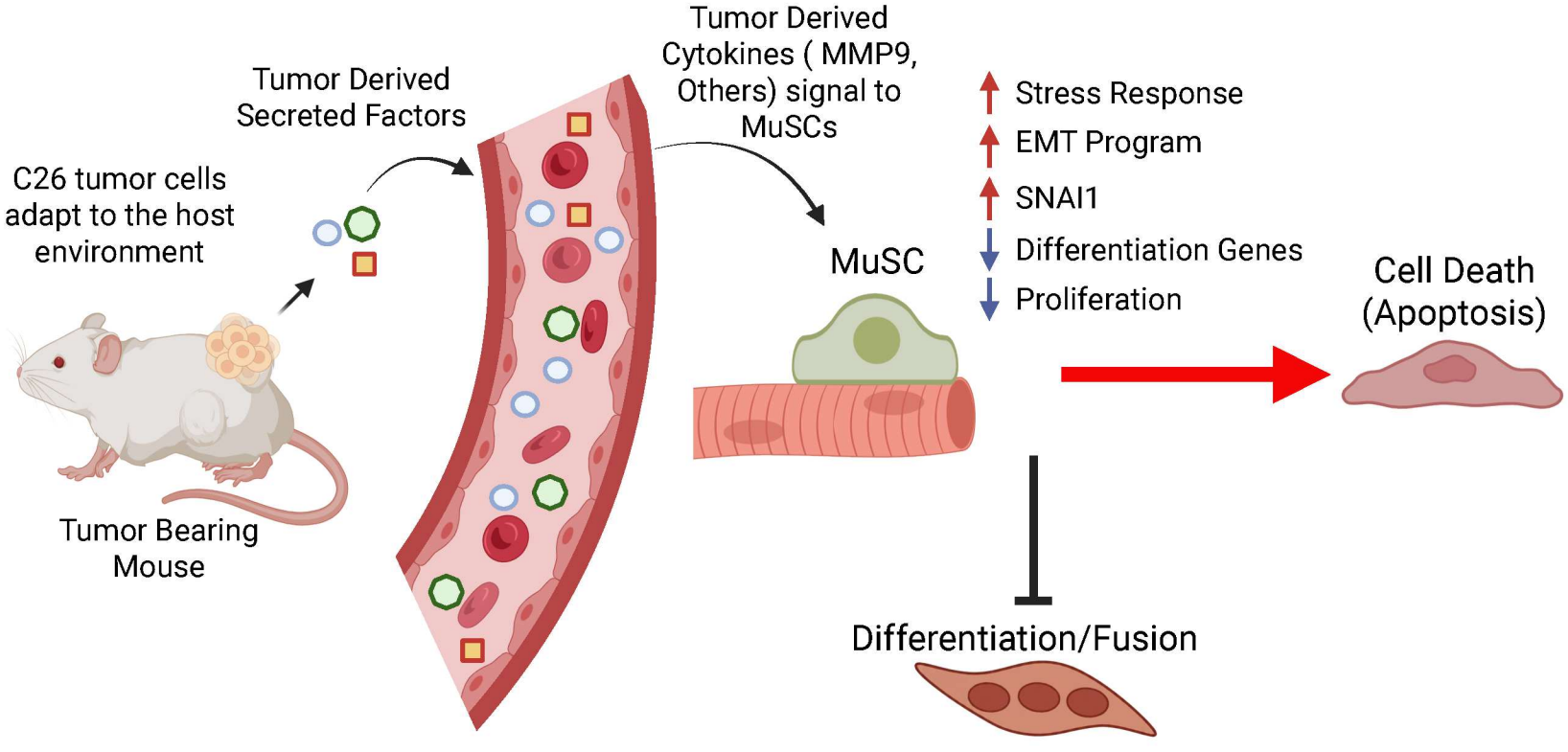

A
EDL MuSC #
Average # of MuSC/Myofiber
p=0.0004680
p=0.002888
p=0.6665
No Tumor
Crispr Control
GDF15 KO
C
TA MuSC #
MuSCs/mm2
p=0.0003366
p=0.0002721
p=0.8695
D
No Tumor
Crispr Control
GDF15 KO
Merge
PAX7
Laminin
DAPI
0 hr EDL Myofibers
B
E
Tumor Free Mass
Weight (g)
p=0.04118
DMSO
JNJ0966
F
Tumor Mass
p=0.7233
G
TA mass
Percent of Total Body Mass
p=1.817e-005
H
7 DPI TA Mass
p=0.1102
I
CSA (μm²)
JNJ0966 Uninjured
Percentage
J
DMSO 7DPI
JNJ0966 7DPI
K
CSA (μm²)
JNJ0966 7DPI
L
EDL #MuSCs
MuSCs/Myofiber
6.995e-006
M
N
TA MuSC#
p=9.385e-011
p=0.0001624
Uninjured
7 DPI
O
Uninjured
7DPI

Figure 9


C26 tumor cells adapt to the host environment
Tumor Derived Secreted Factors
Tumor Derived Cytokines (MMP9, Others) signal to MuSCs
Tumor Bearing Mouse
MuSC
Stress Response
EMT Program
SNAI1
Differentiation Genes
Proliferation
Cell Death (Apoptosis)
Differentiation/Fusion

Supplementary Files

This is a list of supplementary files associated with this preprint. Click to download.

- SupFigure1.tif
- SupFigure2.tif
- SupFigure3.tif
- SupFigure4.tif
- SupFigure5.tif
- SupFigure6.tif
- SupFigure7.tif
- SupFigure8.tif
- SupFigure9.tif
- SupFigure10.tif